Proiectul P1: Caracterizarea mecanică a materialelor celulare și a structurilor sandwich cu miez din materiale celulare folosite la fațade inteligente

Parteneri: **Universitatea Politehnica Timișoara (Coordonator)**
Universitatea Tehnică de Construcții București, UTCB (P1)
Universitatea Tehnică Cluj Napoca (P2)

1.4.1 Influenta temperaturii de testare asupra comportamentului la impact al spumelor metalice compozite

Introducere

Materiale inginerești de înaltă performanță care pot rezista la temperaturi ridicate de funcționare sunt necesare pentru o gamă largă de aplicații critice din diverse industrii [1]. În urma cererii continue de reducere a greutății componentelor structurale, materialele celulare cu matrice metalică [2], polimerică [3] sau ceramică [4] reprezintă o alternativă promițătoare. Comparativ cu alte tipuri de materiale celulare [5], datorită proprietăților lor unice care pot fi atinse prin controlul microstructurii sau al distribuției porilor, spumele metalice sunt materialele ideale [6]. Pe baza structurii lor speciale, spumele metalice constau dintr-o rețea 3D de pori distribuiți stocastic, cu potențialul de a realiza o construcție ușoară și de a îmbunătăți performanțele de rezistență la impact. Toate aceste caracteristici controlabile și ușor previzibile duc la utilizarea spumelor metalice pe scară largă în aplicațiile inginerești unde este necesara o absorbție mare de energie [7].

Utilizarea principală a spumelor metalice este sub sarcini de compresiune și în special în condiții de impact [8]. Majoritatea lucrărilor publicate cu privire la răspunsul la strivire prin compresiune s-au concentrat pe sarcini cvasi-statice [9], în timp ce studiile de impact sunt semnificativ reduse [10]. Mai mult, majoritatea acestor studii la impact au fost efectuate la temperatura camerei. Cu toate acestea, datorită unei sensibilități ridicate la schimbările de temperatură, nu trebuie neglijat efectul temperaturii de testare asupra comportamentului la compresiune al spumelor metalice. Linul și colab. [11, 12], Cady și colab. [13], Yu [14], Fiedler și colab. [15], au investigat efectul temperaturii criogenice asupra proprietăților spumei (rezistența la compresiune și absorbția energiei), în condiții de testare cvasi-statice. Indiferent de tipul de spumă utilizată (spume metalice obișnuite [11, 13], spume metalice sintactice [15], spume metalice ranforsate [11] sau spume poliuretanice [12, 14]), autorii au observat o îmbunătățire a proprietăților pe măsură ce temperatura de testare scade. De exemplu, Linul și colab. [11] au raportat că proprietățile cvasi-statice ale spumelor metalice obișnuite cresc cu 42,91% (rezistența la compresiune), respectiv 49,40% (absorbția energiei) cu scăderea temperaturii de testare de la 25 la -196°C. Autorii au observat aceeași tendință pentru spumele ranforsate, evidențiind o creștere de peste 44% pentru ambele proprietăți. Proprietățile cvasi-statice și dinamice/de impact ale spumei ALPORAS sunt prezentate de Cady și colab. [13] la diferite temperaturi de testare (-196, -100 și 22°C). Autorii au descoperit că rezistenta la compresiune prezintă o dependență ridicată de

temperatura de testare, crescând de la 2,0 MPa (22°C) la 3,6 MPa (-196°C). Mai mult decât atât, comparativ cu temperatura camerei, a fost obținută o creștere cu 70% a performanțelor energiei de absorbție ale spumei atunci când aceasta a fost expusă la temperaturi de testare scăzute. Recent, Fiedler și colab. [15] au investigat comportamentul la compresiune și proprietățile mecanice ale spumelor metalice sintactice A356 și ZA27, tratate și netratate, la temperatura de criogenare. Analiza lor arată o fragilitate semnificativă a spumelor, cu un efect mai pronunțat pentru matricea ZA27. Comparativ cu temperatura camerei, la temperatura de criogenare a fost observată o creștere a rezistentei la compresiune şi a energiei de absorbție. Tratamentul termic (aplicat pentru a crește ductilitatea matricei) nu s-a dovedit a aduce o îmbunătățire semnificativă a proprietăților spumei ZA27, în timp ce s-a obținut o îmbunătățire distinctă a performanței la temperatura de criogenare pentru spumele A356.

Pe de altă parte, principalele proprietăți fizice și mecanice în cazul temperaturilor de testare ridicate au fost raportate la spume metalice obișnuite [16], la spume metalice sintactice [17] și la spume metalice ranforsate [18]. Rezultatele lor arată că creșterea temperaturii de testare afectează în mod semnificativ toate proprietățile spumelor. Aceste modificări ale proprietăților sunt atribuite diferitelor mecanisme de cedare (tranziție fragil-ductil) care au loc în probe odată cu creșterea temperaturii. Rezultatele lui Aakash și colab. [19] indică o tendință liniară de creștere a tensiunilor de curgere/platou și a tensiunii de densificare cu creșterea temperaturii de testare (20, 150, 200, 250 și 300°C). Wang și colab. [20] au observat o creștere a sensibilității la viteză pe măsură ce temperatura de testare crește de la 25 la 500°C, în timp ce Movahedi și colab. [21] au menționat o degradare liniară a tensiunii de platou și a energiei de absorbție pe măsură ce temperatura de testare crește (25, 150 300 și 450°C). Mai mult, Linul și colab. [16] au investigat efectul combinat al temperaturii (25, 150, 300 și 450°C) și al anizotropiei (încărcare axială și laterală) asupra comportamentului la compresiune al spumelor cilindrice de aluminiu cu celule închise și au constatat că temperaturile ridicate evidențiază un efect semnificativ de degradare. Proprietățile la compresiune ale spumelor metalice sintactice au fost investigate de Taherishargh și colab. [17] în intervalul 25-500°C. Autorii au observat că rigiditatea/rezistenta la compresiune și energia de absorbție ale probelor scad semnificativ odată cu creșterea temperaturii. În plus, a fost raportată o variație liniară cu temperatura a capacității de absorbție a energiei spumelor sintactice. Yang și colab. [18] au evaluat proprietățile mecanice la temperatură ridicată al spumelor metalice compozite armate cu nanotuburi de carbon crescute in situ. Autorii au observat că atât rezistenta la compresiune, cat si energia de absorbție scad odată cu creșterea temperaturii de testare (de la 25 la 250°C), dar cresc odată cu creșterea conținutului nanotuburi de carbon. De asemenea, au descoperit că, la 25°C, tensiunile de curgere şi de platou ale spumelor compozite sunt de aproximativ 1,6, respectiv 0,8 ori mai mari decât cele al spumei de aluminiu pur.

După cum s-a menționat de către Yang și colab. [18], Taherishargh și colab. [17] Linul și colab. [11], Orbulov și colab. [22] și Katona și colab. [23], utilizarea diferitelor armături pentru spume metalice compozite de înaltă rezistență sunt cruciale pentru a optimiza răspunsul la compresiune al acestora. Prin urmare, această lucrare investighează comportamentul la compresiune dinamică al spumelor metalice neranforsate și ranforsate, în condiții termomecanice

extreme (temperaturi ridicate și viteze de încărcare diferite). Mai mult, mecanismele de cedare ale probelor sunt discutate împreună cu o analiză microstructurală a spumelor. În plus, se fac comparații între datele dinamice și cvasi-statice în ceea ce privește proprietățile de rezistență și performanțele energiei de absorbție, în intervalul 25-350°C.

Comportamentul la impact

Curbele forță - deplasare au fost colectate în timpul testelor experimentale de către software-ul conectat la mașina de testare și au fost convertite în curbe tensiune și deformație. Figura 1 prezintă curbele tensiune-deformație ale spumelor investigate.

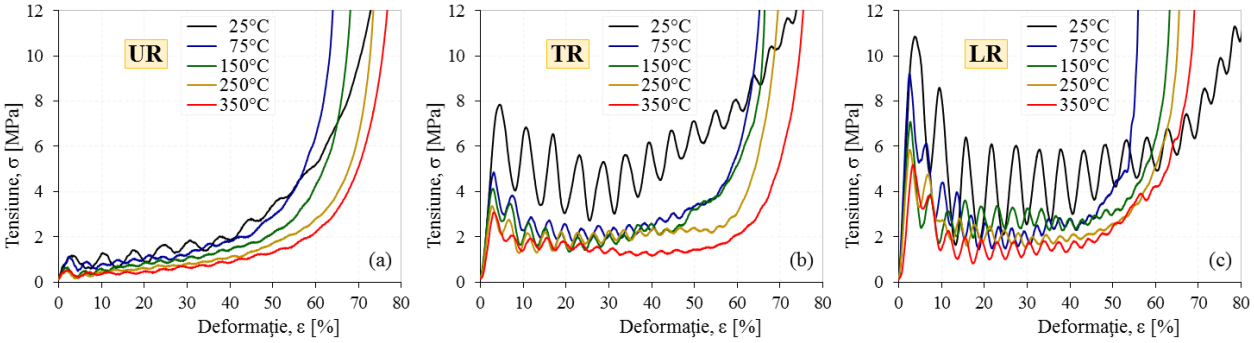

Fig. 1. Influenţa temperaturii de testare asupra comportamentului la compresiune dinamică al spumelor metalice neranforsate (A) şi ranforsate (b, c)

Comportamentul la compresiune al spumelor investigate este similar cu majoritatea materialelor celulare. Din Fig. 1, se observă că spumele testate prezintă trei regiuni caracteristice: regiunea liniar-elastic, de platou și regiune de densificare. Rigiditatea efectivă a spumei este obținută din panta primei regiuni liniare, în timp ce rezistența la compresiune a spumei este dată de sfârșitul primei regiuni unde este identificat primul maxim din curba tensiune-deformație. Se poate observa că toate curbele prezintă un punct maxim vizibil și ușor de identificat. În cazul materialelor celulare (spume metalice, polimerice și de sticlă), rezistența la compresiune este asociată cu tensiunea de curgere. Scăderea inițială a tensiunii între regiunile elastice și de platou este marcată de apariția primei benzi de deformare în epruveta. Tensiunea de platou se determină ca medie aritmetică între tensiunile corespunzătoare unor deformații de 20%, respectiv 40%. Forma și dimensiunea zonei platoului pot fi controlate de mecanismele de cedare care apar în timpul testelor de comprimare (de exemplu cedarea / flambarea / îndoirea / ruperea pereților celulelor), de tipul de spumei (spume ranforsate / neranforsate, spume cu celule închise / deschise) , etc.) și de condițiile de testare (temperatură scăzută / camerei / ridicată, teste de impact / cvasi-statice etc.). În acest caz, mecanismele de deformare dominante care au afectat forma curbelor tensiune-deformație au fost guvernate de condițiile de încărcare și de temperatura de testare.

Proprietățile la impact

Figura 2 prezinta variația principalelor proprietăți mecanice (tensiunea de curgere, tensiunea de platou, tensiunea de densificare şi energia de absorbție la densificare) în funcție de

tipul spumei (spuma neranforsată, spuma ranforsată longitudinal/transversal) şi temperatura de testare. Rezultatele din Fig. 2 arată că, comparativ cu spumele neranforsate, utilizarea armăturilor duce la o creștere a proprietăților spumelor cu până la 8,5 ori. Această diferență rămâne aproape constantă pentru toate temperaturile de testare. În ceea ce privește cele două tipuri de armături, spumele ranforsate longitudinal evidențiază o rezistență la compresiune mai mare decât spumele ranforsate transversal.

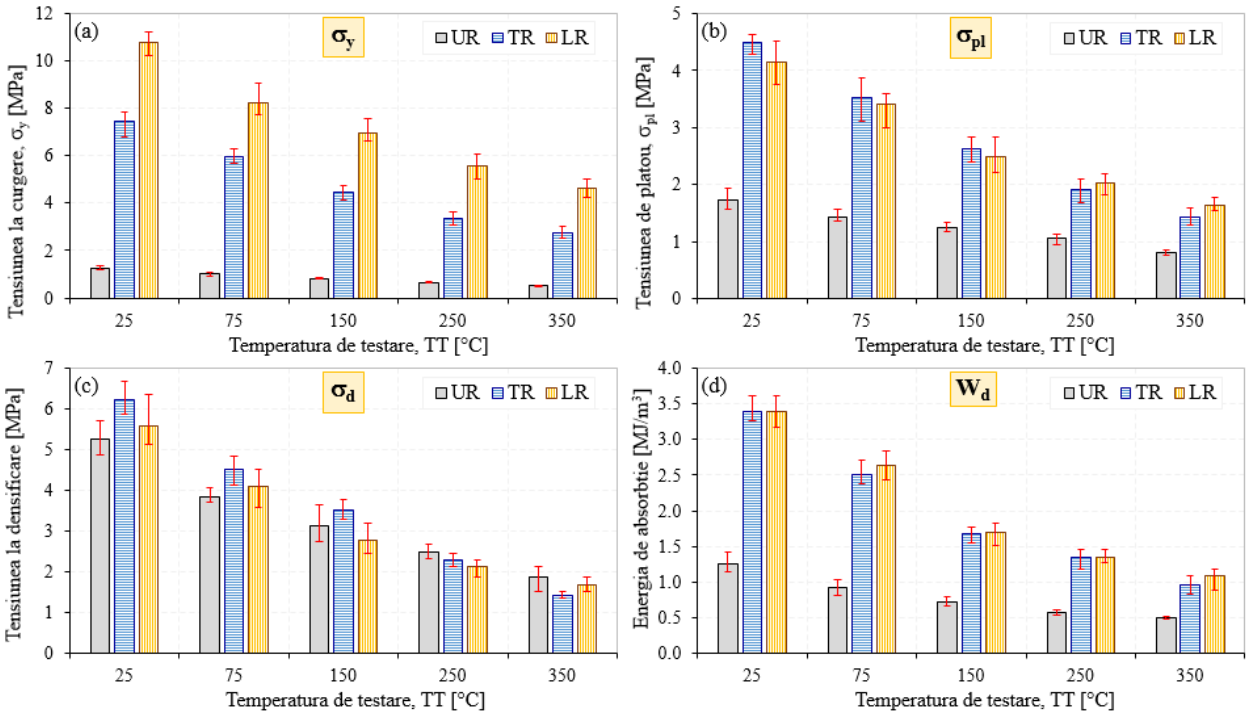

Fig. 2. Variația tensiunii de curgere, de platou, de densificare şi a energiei de absorbție cu temperatura de testare

Analiza microstructurală

Toate probele investigate au prezentat mecanisme de deformare progresivă. Figura 3 prezinta imaginile microstructurii spumelor obținute la același ordin de mărire (10x). La temperatura camerei spumele prezintă o matrice fragilă, aceasta schimbând-se în una ductilă odată cu creșterea temperaturii de testare pana la 350°C. Matricea fragila permite inițierea şi propagarea microfisurilor, în timp ce matricea ductilă conduce la o deformare plastică a pereților celulelor.

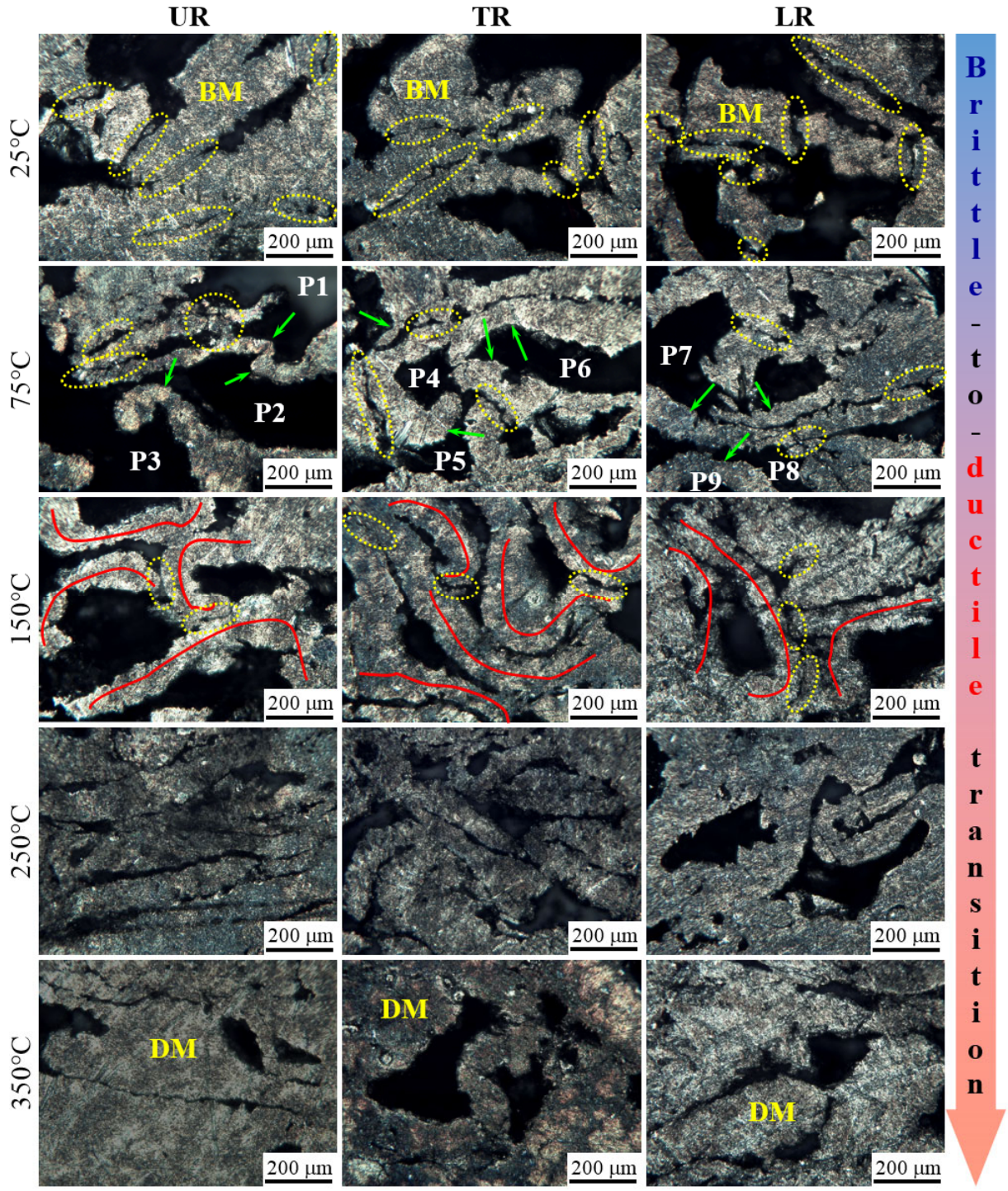

Fig. 3. Imagini microstructurale cu epruvetele deformate

Comparație static-impact

Figura 4 ilustrează o comparație static-impact a curbelor tensiune-deformație la temperatura camerei. Au fost făcute comparații la toate temperaturile utilizate pentru testele de impact (25, 75, 150, 250 și 350 ° C), dar pentru a evita repetarea graficelor, au fost prezentate doar curbe la 25°C, celelalte temperaturi urmând aceleași tendințe.

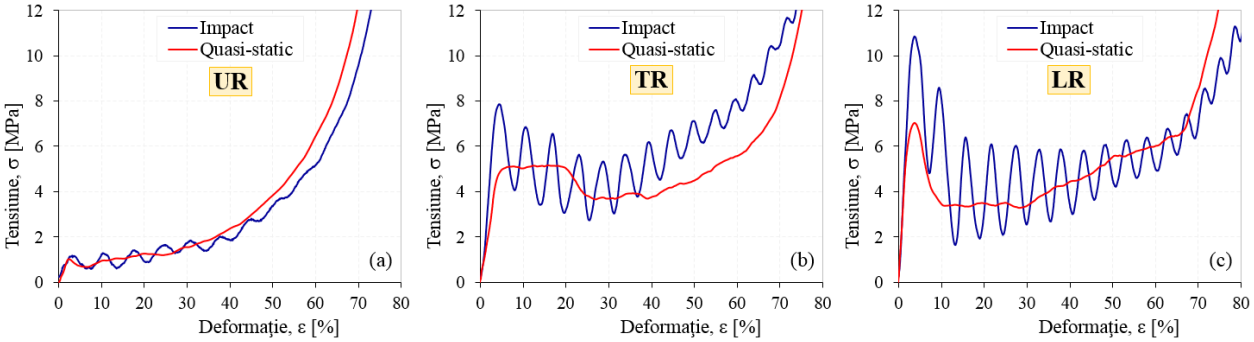

Fig. 4. Comparație a curbelor tensiune-deformație

Cele două tipuri de teste arată comportamente foarte diferite în ceea ce privește curbele tensiune-deformație. În cazul testelor cvasi-statice, din cauza lipsei oscilațiilor mari, atât regiunea platoului, cât și începutul densificării sunt mai evidente. În general, în condiții de impact, materialul matricei se comportă mai fragil în comparație cu cvasi-static, datorită schimbării bruște a mecanismelor de cedare.

Figura 5 prezintă valorile măsurate ale rezistenței la compresiune ale probelor obținute prin teste de impact și de compresiune cvasistatică. Indiferent de tipul testului, aceste valori scad odată cu creșterea temperaturii de testare.

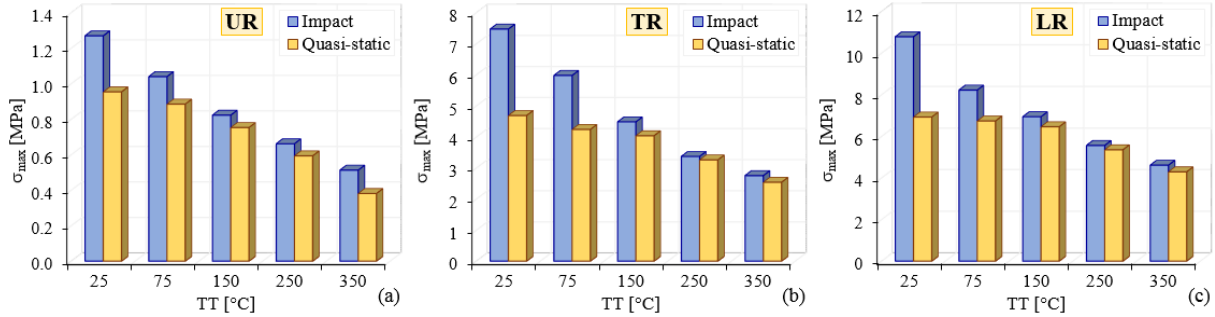

Fig. 5. Comparatie static-impact a rezistentei la compresiune

Testele efectuate la viteze mari de încărcare prezintă proprietăți mecanice mai bune. Diferența majora este obținută la temperatura camerei, rezultatele apropiindu-se odată cu creșterea temperaturii de testare.

1.4.2 Caracterizarea mecanică a spumelor ceramice

Proprietățile mecanice ale ceramicii poroase sunt puternic influențate de microstructura lor. Prin urmare, comportamentul mecanic al ceramicii foarte poroase este diferit de cel al ceramicii. În această lucrare, evaluăm diferite metode de testare mecanică, ar fi compresie, testul discului brazilian și îndoirea în 3 puncte a adecvării acestora pentru compararea materiale ceramice poroase. Se arată că îndoirea în 3 puncte este mai potrivită decât compresie sau testarea discului brazilian, deoarece materialul nu prezintă nicio propagare critică a fisurilor în încărcare compresivă. Cu încercări de îndoire în 3 puncte, o comparație cantitativă a proprietățile spumelor cu diferite microstructuri și porozități este posibilă.

Spumele ceramice combină substanțe chimice ridicate și stabilitate termică ridicată cu conductivitate termică scăzută și suprafață ridicată. Prin urmare, acestea sunt candidați ideali în domeniul izolației la temperaturi ridicate și pentru catalizatoare , suporturi sau filtre pentru metale topite. În ceramica poroasă, dimensiunii și distribuția dimensiunii, precum și interconectivitatea și textura porilor joacă un rol important, deoarece determina proprietăți precum rezistența mecanică, rezistența termică, conductivitatea și permeabilitatea gazelor și lichidelor. Microstructura ceramicii poroase este controlată de calea de procesare și parametrii corespunzători acestora. Există multe căi de prelucrare a ceramicii poroase; cele mai multe dintre ele pot fi grupate în oricare dintre următoarele metode: În metoda replicării, un burete polimeric este impregnat cu o suspensie ceramică, iar după arderea organică, o spuma cu celule deschise este obținută în cazul în care dimensiunea celulei este determinată de structura spumei șablon. În metoda fazei fugare, se utilizează un por de sacrificiu care duce adesea la spume cu structuri poroase foarte ordonate după îndepărtarea porilor anteriori. În metoda fazei fugare, se utilizează un por de sacrificiu care duce adesea la spume cu structuri poroase foarte ordonate după îndepărtarea porilor anteriori. În spumarea directă, o faza este dispersată și stabilizată într-un lichid și atât structurile celulare deschise, cât și cele închise pot fi obținute după uscare și sinterizare, în funcție de diferiți parametri de prelucrare. Comună tuturor metodelor, porozitatea introdusă va afectează și modifică proprietățile mecanice ale materialelor într-un fel sau altul.

Ca urmare a acestei schimbări în comportamentul mecanic, unele tehnici de măsurare mecanică aplicate în mod obișnuit pentru ceramica densă ar putea să nu fie la fel de potrivite pentru ceramica poroasă. Influența porozității asupra rezistenței mecanice a fost studiat în detaliu, Gibson și Ashby [24] au prezentat un model pentru a descrie această influență. În modelul lor de "grinzi și bare" ei descriu legătura dintre porozitate și diverse proprietăți mecanice ale ceramicii celulare cu structuri cu celule deschise și închise. Conform acestui model, nici o influență a dimensiunii celulelor nu trebuie așteptat. În timp ce Dam et al.8 a observat o creștere a rezistenței mecanice cu creșterea dimensiunii celulelor în studiul lor privind alumina mullite, Brezny și Green [25] au arătat că acest efect nu a fost prezent în carbonul vitros reticulat și au concluzionat că schimbarea rezistenței mecanice a materialului mullit de alumină s-a datorat mai degrabă unei modificări a microstructurii strut și dimensiunii critice a defectelor decât efectelor dimensiunii celulelor. O mare varietate de metode de testare mecanică poate fi utilizate pentru a măsura comportamentul unui material sub

diferite solicitări. Cu toate acestea, aceste metode de testare nu au fost concepute special pentru ceramica foarte poroasă, cu o arhitectură tridimensională a porilor, iar comportamentul acestor materiale în diferite condiții de încărcare nu a fost studiat în detaliu. O atenție deosebită trebuie acordată porilor și dimensiunii acestora. Deoarece porii de la interfața cu aparatul de testare reduc contactul tensiunile sunt concentrate în lamelele spumoase. În plus, porii de la suprafața eșantionului pot servi ca puncte de inițiere a fisurilor. În acest studiu, investigăm răspunsul aluminei poroase la încovoiere în 3 puncte, compresiune și tensiune indirectă folosind metoda discului brazilian. Aceste metode au fost alese datorită simplității în pregătirea specimenelor și a configurațiilor ușoare de măsurare și reprezintă o varietate de moduri diferite de încărcare. O imagine reprezentativă a epruvetele și configurațiile de măsurare sunt prezentate în Fig. 6, [26].

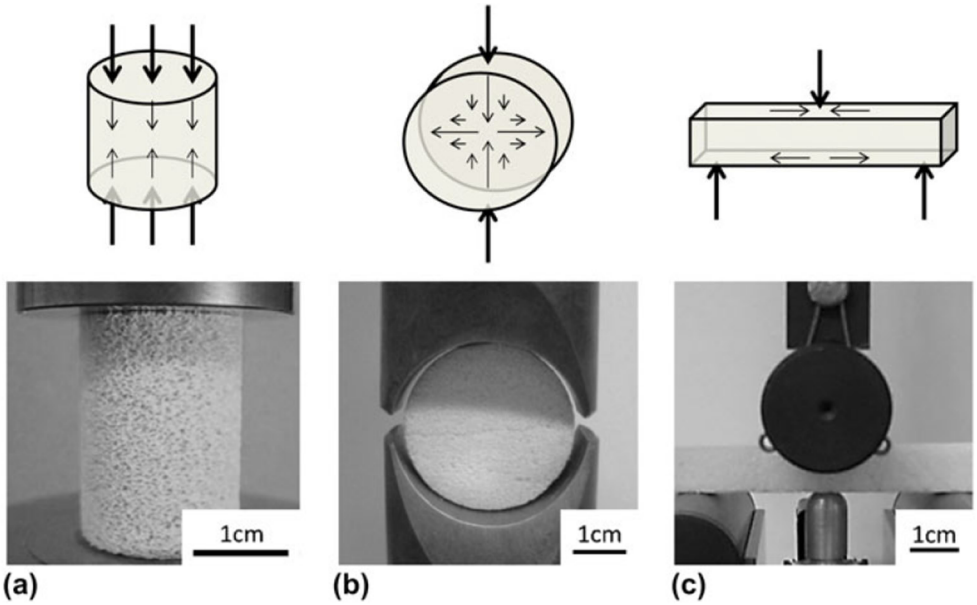

Fig. 6 Cele trei metode diferite de testare mecanică utilizate a spumelor ceramice: (a) compresine (b) testarea discului brazilian (c) încercarea de încovoiere în 3 puncte.

La metoda discului brazilian, o probă cilindrică este comprimată în direcție radială, rezultând o combinație de forțelor de tracțiune într-un volum mare în interiorul mostră. În general, această metodă oferă avantajul importanței reduse a finisajului suprafeței eșantionului și, prin urmare, reproductibilitate potențial mai bună în comparație cu alte metode. În îndoire în 3 puncte, un eșantion dreptunghiular este plasat pe două suporturi și încărcat din partea de sus cu un al treilea sprijin la mijloc, ceea ce duce la forțe de tracțiune în partea inferioară și forțele compresive din partea superioară a eșantionului. În acest studiu, evaluăm diferite metode de testare mecanică privind adecvarea și valoarea informativă a acestora pentru compararea ceramicii poroase. Materialul de testare utilizate aici a fost produsă prin spumarea directă a suspensii concentrate de alumină. Aerul introdus este

stabilizat de particule de alumină in situ-hidrofobizate și active la suprafață, ceea ce duce la spume cu stabilitate în stare umedă, care sunt apoi prelucrate în ceramică poroasă.

Tehnologia de fabricație a spumelor

În cadrul determinarilor experimentale au fost utilizate două produse ale firmei Dentsply Prosthetics : Ceramco Dentin și Ceramco Enamel , continand , conform fisei tehnice, aluminosilicati de sodiu si potasiu cu compoziţia între 80-100 % şi SnO2 între 0-20% conform fişei tehnice.

Masele vitroceramice au fost obținute după schema prezentată in Fig. 7.

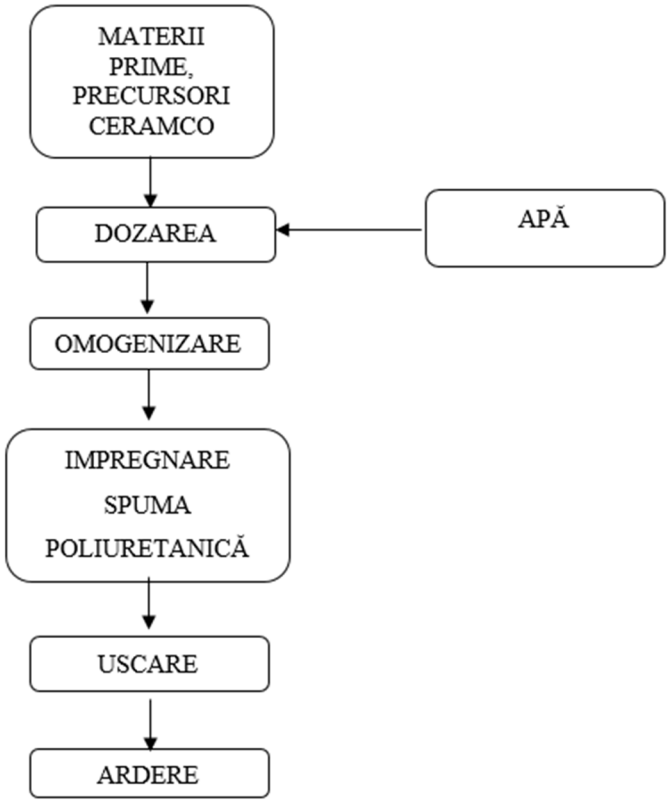

Fig. 7 Fluxul tehnologic de obținere a produselor bioceramice

Porţelanul folosit are compoziţia prezentată în Tabelul 1

Tab. 1 Compoziția portelanului folosit

Materie prima	**Compozitie [% grav.]**
Caolin	47
Feldspat	28.5
Nisip	24.5

Au fost folosiţi bureţi proveniti de la S.C. Spumotim S.A. având densitaţiile de 210, 250 și respectiv 300 kg/m^3. Bureţii au fost folosiţi sub formă de cuburi cu latura de 2 cm. Impregnarea s-a realizat în barbotina timp de 30 de secunde. După aceasta, probele au fost uscate imediat la temperatura de 120° C timp de 24 ore.

Tratamentul termic realizat într-un cuptor electric s-a realizat in două faze: prima la temperatura de 450°C pentru arderea fazei organice şi a doua la temperatura 750° C și respectiv 1000° C pentru porţelan timp de o oră.

Porozitatea maselor bioceramice

Porozitatea totală în procente volumetrice s-a calculat cu formula:

$$P = \left(1 - \frac{M_p}{M_t}\right) \cdot 100 \ (\%) \qquad (1)$$

unde : M_p = masa probei,

M_t = masa teoretică.

Masa teoretică se calculează înmulțind volumul probei cu densitatea teoretică a porțelanului 2,35 g/cm^3.

Valoarea porozității probelor arse la cele 2 temperaturi este prezentată în Tabelul 2

Tab. 2 Porozitatea aparentă a materialelor obținute

Proba	Temperatura de ardere (° C)	P_{tot} [%]	Densități burete [kg/m^3]
1	1000	51.69	210
2		60.23	250
3		65.85	300
4	750	75.15	210
5		79.92	250
6		83.48	300

Se observă că porozitatea materialului este influențată pe de-o parte de densitatea spumei poliuretanice precursoare și, pe de altă parte de temperatura de ardere. Creșterea densității buretelui duce, prin arderea acestuia la spume mai poroase. O temperatură de tratament termic mai mare generază în masa de porțelan mai multă fază lichidă – topitură – care va umple porii și, ca urmare va duce la o scădere a porozității materialului.

Compoziția fazală a maselor bioceramice

Natura fazelor prezente în structura maselor studiate a fost investigată folosind un difractometru de RX tip Rigaku Ultima 4.

Rezultatele obținute pentru probele sintetizate sunt prezentate în fig. 8 și 9.

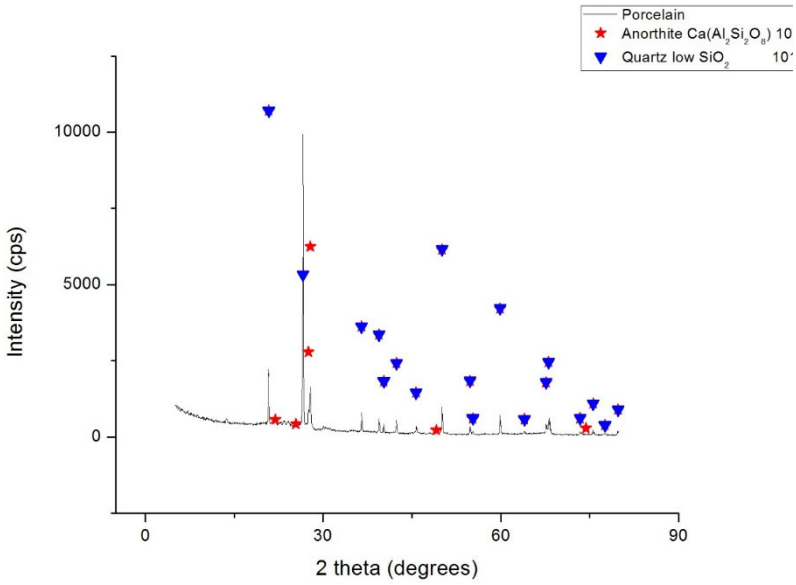

Fig. 8 Compoziția fazală a masei obținute din porțelan, după ardere

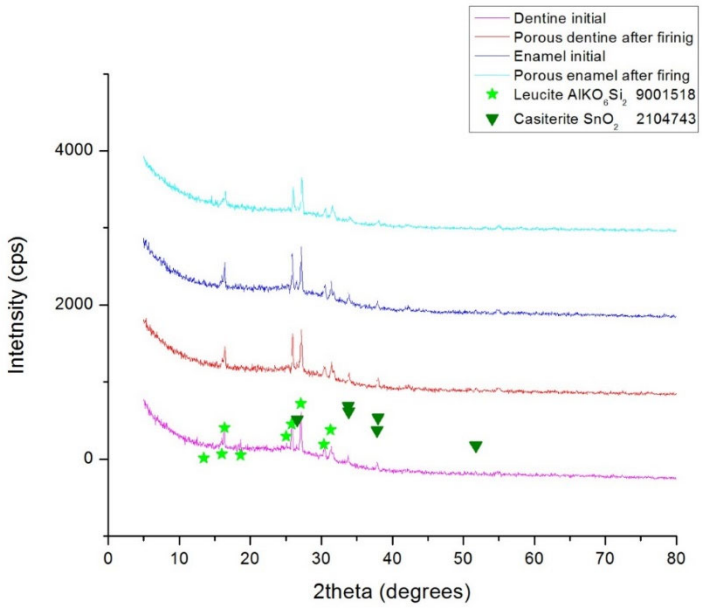

Fig. 9 Compoziția fazală a probelor obținute din dentină și email, înainte și după ardere

Morfologia structurală

Setul de probe obținute plecând de la buretele cu densitate 210 kg/m^3 sunt prezentate în figura 10

Fig. 10 Setul de probe obținut plecând de la buretele având densitatea 210 kg/m^3

Un aspect inovator al metodei de obținere folosite este legat de posibilitatea obținerii unei structuri comparabile cu cea a osului biologic având atât o zonă mediană poroasă cât și zona periferică (periost) compactă și dură așa cum se observă în fig. 11.

Fig. 11 Structura materialului sintetizat în secțiune transversal

Rezistența la compresiune a spumelor ceramice

Compresiunea este unul dintre solicitările cele mai frecvente la care materialul bioceramic este supus în aplicațiile reale. Tensiunea la compresiune s-a calculat cu formula:

$$\sigma = \frac{F}{S} \text{ [MPa]}$$

unde : F = forța maximă de compresiune [N],

S = suprafața probei [mm^2].

Pentru calculul rezistenței la compresiune a fost măsurată forța de distrugere prin compresiune pe o presă Zwick/Roell Z005, Fig. 12.

Fig. 12 Rezistența la compresiune a maselor sintetizate

Tab. 3 Rezultatele testelor de compresiune

	Masa	Dimensiunile probei			Volum	Densitate	Forta maxima	Rezistenta la compresiune
proba	m [g]	h [mm]	l1 [mm]	l2 [mm]	V [cm^3]	ρ [g/cm^3]	Fmax [N]	σ [MPa]
1_1		22	23.2	22	11.229		560	1.10
1_2		20.3	25	23	11.672		1470	2.56
1_3		22.6	20.8	23	10.812		230	0.48
2.1	12.6	21.72	21.36	25.37	11.770	1.070	717	1.32
2.2	9.7	23.04	21.33	21.06	10.349	0.937	140	0.31
2.3	8.6	22.6	23.1	22.6	11.798	0.729	161	0.31
3.1	13.6	23.94	20.62	23.36	11.531	1.179	1420	2.95
3.2	10.5	21.77	21.22	22.57	10.426	1.007	135	0.28
3.3	12.4	21.35	22.29	26.27	12.502	0.992	377	0.64
4.1	8.9	20.23	19.15	23.94	9.274	0.959	90	0.20
4.2	11.84	21.32	21.03	24.03	10.774	1.099	607	1.20
4.3	10.6	19.58	21.84	24.03	10.276	1.031	444	0.85
5.1	11.63	24.9	22.78	21.48	12.184	0.954	494	1.01
5.2	10.21	24.58	21.13	19.21	9.977	1.023	564	1.39
5.3	9.9	21.55	23.04	22.78	11.310	0.875	555	1.06
6.1	10.07	20.29	19.32	23.69	9.286	1.085	160	0.35
6.2	10.2	23.84	22.21	21	11.119	0.917	205	0.44
6.3	10.75	23.51	21.17	22.34	11.119	0.967	224	0.47

Probele au fost cântărite și măsurate înainte de efectuarea testelor de compresiune, aflând astfel masă (g) , înălțimea(h) și dimensiunile transversale ale probelor (l1/l2)

Valoarea rezistențelor la compresiune ale probelor studiate sunt prezentate în Tabelul 3 și ilustrate grafic în Fig. 13. Se observă că, pentru ambele temperaturi de ardere, probele prezintă o scădere a rezistenței la compresiune odată cu creșterea porozității probelor studiate.

De asemenea, temperatura de ardere mai mare de 1000^0 C conferă o rezistență la compresiune mai mare.

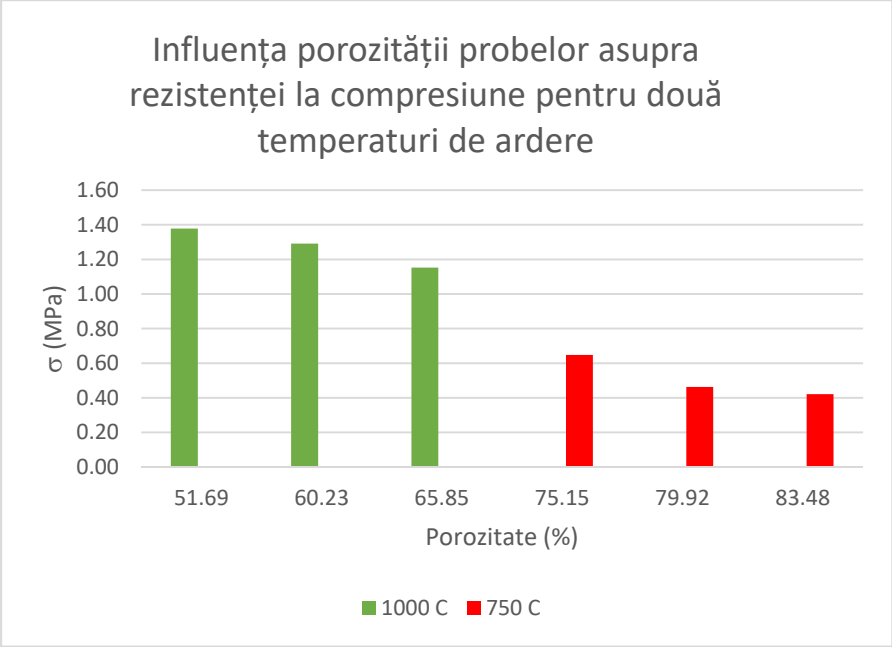

Fig. 13 Efectul porozității asupra rezistenței la compresiune

Tab. 4 Comparatie a rezultatelor testelor de compresiune

Proba	P_{tot} [%]	Rezistența la compresiune [MPa]	
		1000^0 C	750^0 C
1	51.69	1.38	
2	60.23	1.29	
3	65.85	1.15	
4	75.15		0.65
5	79.92		0.46
6	83.48		0.42

Concluzii

- S-au realizat teste de compresiune pe spume metalice neramforsate și ramforsate în domeniul de temperatură 25 – 350^0 C în regim static și dinamic.
- Rezultatele testelor statice indică o scădere a propietăților la compresiune cu creșterea temperaturi, Fig. 2 și 6.
- Aceiași tendință de scădere a proprietăților mecanice cu creșterea temperaturii se observă și la testele de impact, Fig. 6.
- Proprietățile la impact sunt mai mari decât cele obținute în condiții statice pentru toate cele trei tipuri de epruvete considerate., indicând o capacitate ridicată de absorbție a energiei de impact a acestor materiale, Fig. 6.
- Ranforsarea epruvetelor din spumă de aluminiu cu plasa din oțel produce o creștere semnificativă a proprietăților mecenică: limita de curgere, tensiunea de platou și energia de absorbție. Principlaele rezultate au fost publicate in Jurnalul Composites A [27], articol anexat.

- Spumele ceramice sunt spume dure realizate din ceramică sau ceramică cu structură asemănătoare spumei. Este un fel de ceramică poroasă cu porozitate ridicată și uneori numită ceramică celulară. Datorită cantității mari de pori și suprafață, spumele ceramice sunt potrivite în special pentru filtrarea metalelor topite sau a gazelor fierbinți, a sistemelor de protecție termică și a schimbătoarelor de căldură.
- Printre aplicațiile spumelor ceramice se enumeră și aplicațiilele biomedicale, s-a descoperit că substanțe osoase și implanturi resorbabile pot fi produse atunci când hidroxiapatita și alte variante de fosfat de calciu sunt utilizate că fază ceramică.
- S-a studiat influența porozității suportului poliuretanic asupra structurii ceramicii obținute.
- Testele la compresiune au confirmat rolul jucat de porozitate asupra proprietăților materialelor obținute. Acestea au valori ale efortului la compresiune sensibil mai mici comparativ cu datele din literatură însă este dificila realizarea unei comparații între materiale din cauza porozității diferite a acestora.

Bibliografie

[1] Maiorano LP, Molina JM. Guiding heat in active thermal management: One-pot incorporation of interfacial nano-engineered aluminium/diamond composites into aluminium foams. Compos Part A 2020;133:105859.

[2] Ashby MF, Evans A, Fleck NA et al. Metal Foams: A Design Guide. Butterworth-Heinemann, USA, 2000.

[3] Zhou T, Zhang P, Xiao W, et al. Experimental investigation on the performance of PVC foam core sandwich panels under air blast loading. Compos Struct 2019;226:111081.

[4] Xu Z, Duan L, Hou Y, et al. The influence of carbon-encapsulated transition metal oxide microparticles on reducing toxic gases release and smoke suppression of rigid polyurethane foam composites. Compos Part A 2020; 131:105815.

[5] Pietras D, Linul E, Sadowski T, Rusinek A. Out-of-plane crushing response of aluminium honeycombs in-situ filled with graphene-reinforced polyurethane foam. Compos Struct 2020;249:112548.

[6] Sun G, Wang Z, Yu H, et al. Experimental and numerical investigation into the crashworthiness of metal-foam-composite hybrid structures. Compos Struct 2019;209:535-547.

[7] Huo X, Sun G, Zhang H, et al. Experimental study on low-velocity impact responses and residual properties of composite sandwiches with metallic foam core. Compos Struct 2019;223:110835.

[8] Liu H, Ding S, Ng BF. Impact response and energy absorption of functionally graded foam under temperature gradient environment. Compos Part B-Eng 2019;172:516-532.

[9] Wejrzanowski T, Cwieka K, Skibinski J, et al. Metallic foam supported electrodes for molten carbonate fuel cells. Mater Des 2020;193:108864.

[10] Sahu S, Mondal DP, Cho JU, et al. Low-velocity impact characteristics of closed cell AA2014-SiCp composite foam. Compos Part B-Eng 2019;160:394-401.

[11] Linul E, Marşavina L, Linul PA, Kovacik J. Cryogenic and high temperature compressive properties of Metal Foam Matrix Composites. Compos Struct 2019;209:490-498.

[12] Linul E, Marşavina L, Vălean C, Bănică R. Static and dynamic mode I fracture toughness of rigid PUR foams under room and cryogenic temperatures. Eng Fract Mech 2020;225:106274.

[13] Cady CM, Gray III GT, Liu C. et al. Compressive properties of a closed-cell aluminium foam as a function of strain rate and temperature. Mater Sci Eng A 2009;525(1-2):1-6.

[14] Yu YH, Choi I, Nam S, Lee DG. Cryogenic characteristics of chopped glass fiber reinforced polyurethane foam. Compos Struct 2014;107:476-481.

[15] Fiedler T, Al-Sahlani K, Linul PA, et al. Mechanical properties of A356 and ZA27 metallic syntactic foams at cryogenic temperature. J Alloys Compd 2020;813:152181.

[16] Linul E, Movahedi N, Marsavina L. The temperature and anisotropy effect on compressive behaviour of cylindrical closed-cell aluminium-alloy foams. J Alloys Compd 2018;740:1172-1179.

[17] Taherishargh M, Linul E, Broxtermann S, Fiedler T. The mechanical properties of expanded perlite-aluminium syntactic foam at elevated temperatures. J Alloy Compd 2018;737:590-596.
[18] Yang K, Yang X, Liu E, et al. Elevated temperature compressive properties and energy absorption response of in-situ grown CNT-reinforced Al composite foams. Mater Sci Eng A 2017;690:294-302.
[19] Aakash BS, Bi S, Shields MD, Gaitanaros S. On the high-temperature crushing of metal foams. Int J Solids Struct 2019;174-175:18-27.
[20] Wang P, Xu S, Li Z. et al. Temperature effects on the mechanical behaviour of aluminium foam under dynamic loading. Mater Sci Eng A 2014;599:174-179.
[21] Movahedi N, Linul E, Marsavina L. The temperature effect on the compressive behaviour of closed-cell aluminium-alloy foams. J Mater Eng Perform 2018;27(1):99-108.
[22] Orbulov IN, Szlancsik A, Kemény A, Kincses D. Compressive mechanical properties of low-cost, aluminium matrix syntactic foams. Compos Part A 2020;135:105923.
[23] Katona B, Szlancsik A, Tábi T, Orbulov IN. Compressive characteristics and low frequency damping of aluminium matrix syntactic foams. Mat Sci Eng A 2019;739:140-148.
[24] Gibson LJ, Ashby MF. *Cellular solids, structure and properties*. Second edition, Cambridge University Press; 1997.
[25] Brezny R, Green DJ, Fracture behavior of open-cell ceramics, J. Amer. Ceramic Society, 1989; 72: 1145-1152.
[26] Seeber B.S.M, Gonzenbach U.T, Gauckler L.J, Mechanical properties of highly porous alumina foams, Department of Materials, J. Mater. Res., 28 (18), 2013, 2281-2287.
[27] Linul E, Pietras D., Sadowski T., Marsavina L, Rajak D.K, Kovacik J, Crashworthiness performance of lightweight Composite Metallic Foams at high temperatures, Composites Part A, Vol. 149, 2021, 106516.

Composites: Part A 149 (2021) 106516

Contents lists available at ScienceDirect

Composites Part A

journal homepage: www.elsevier.com/locate/compositesa

Crashworthiness performance of lightweight Composite Metallic Foams at high temperatures

Emanoil Linul [a,*], Daniel Pietras [b], Tomasz Sadowski [b], Liviu Marşavina [a], Dipen Kumar Rajak [c], Jaroslav Kovacik [d]

[a] Departament of Mechanics and Strength of Materials, Politehnica University of Timisoara, 1 Mihai Viteazu Avenue, 300 222 Timisoara, Romania
[b] Department of Solid Mechanics, Lublin University of Technology, Nadbystrzycka 38, 20-618 Lublin, Poland
[c] Department of Mechanical Engineering, Sandip Institute of Technology and Research Centre, Nashik, MH 422213, India
[d] Institute of Materials and Machine Mechanics, Slovak Academy of Sciences, Dúbravská cesta 9, 845 13 Bratislava, Slovak Republic

ARTICLE INFO

Keywords:
Composite metallic foams
Compressive properties
High temperatures
Collapse mechanisms

ABSTRACT

Based on their special stochastically distributed pores, Composite Metallic Foams (CMFs) represent a promising alternative to the conventional high-density solid structures. However, due to their high sensitivity to temperature changes, the effect of testing temperature on the compression behaviour of CMFs should not be neglected. In this paper, the compressive response of expanded metal mesh (EMM) reinforced metallic foams, manufactured by powder metallurgical route, were evaluated under impact tests (strain rate 95 s^{-1}) as a function of testing temperature (i.e. 25, 75, 150, 250 and 350 °C). The impact properties of high-strength CMFs including strength properties and energy absorption performances, are measured and compared with those obtained under quasi-static (strain rate $5.77 \cdot 10^{-3}$ s^{-1}) loading conditions. The effect of EMM reinforcements on the CMFs properties and collapse mechanisms at the cell-level were discussed according to the testing temperature. The deformation behaviour of the lightweight CMFs was found to be strongly temperature-dependent, highlighting a brittle-to-ductile transition with increasing testing temperature. Finally, based on the quasi-static experimental results, empirical formulae are proposed to predict the impact properties of newly-developed CMFs, i.e. compression strength and energy absorption.

1. Introduction

High-performance engineering materials that can withstand high operating temperatures, without failure or damage, are required for a wide range of critical structural engineering applications in various industries [1–3]. Following the continuous demand for reducing the weight of the structural components, the bio-inspired cellular materials with metallic [4–6], polymeric [7–9] or ceramic [10,11] matrix represent a promising alternative to the conventional high-density solid structures (e.g. steel, aluminium, etc.). Compared to other types of cellular materials [12,13], metallic foams (MFs) are excellent candidates for this purpose due to their unique properties – high stiffness-to-weight ratio, high ability to absorb impact energy, good formability and corrosion resistance, recycling potential, etc. – that can be attained by controlling their microstructure or pore distribution [14–16]. Based on their special structure, MFs consist of a 3D network of stochastically distributed pores with the potential to achieve the lightweight construction and improve the crashworthiness performances. All of these controllable and easily predictable features lead to the use of MFs on a large scale in energy absorptions, impact mitigation and blast protection applications [17,18].

The main use of MFs is under compression loads, and especially under impact conditions [19–21]. Most of the published works on the compressive crushing response were focused on quasi-static loads [22–24], while impact studies are significantly reduced [25–27]. Moreover, the majority of these impact studies were performed at room temperature (RT). However, due to a high sensitivity to temperature changes, the effect of testing temperature (TT) on the compression behaviour of MFs should not be neglected. Linul et al [28,29], Cady et al. [30], Yu [31], Fiedler et al [32], investigated the effect of cryogenic temperatures (CT) on foam properties (compressive strength, σ_{max} and energy absorption, W), under quasi-static testing conditions. Regardless of the type of foam used (regular MFs [28,30], MSFs [32], reinforced MFs [28] or polyurethane foams (PUFs) [29,31]), the authors observed a properties enhancement as TT decreases. For example, Linul et al [28]

* Corresponding author.
E-mail address: emanoil.linul@upt.ro (E. Linul).

https://doi.org/10.1016/j.compositesa.2021.106516
Received 6 February 2021; Received in revised form 27 May 2021; Accepted 3 June 2021
Available online 7 June 2021

Nomenclature

A	Sample cross-sectional area
BM	Brittle Matrix
CaH_2	Calcium hydride
CMF	Composite Metallic Foam
CNT	Carbon nanotube
CT	Cryogenic Temperature
DM	Ductile Matrix
EDM	Electric Discharge Machining
EMM	Expanded Metal Mesh
F	Load
LR	Longitudinal Reinforced
l_0	Sample height
MF	Metallic Foam
MSF	Metallic Syntactic Foam
MWCNTs	Multi-wall carbon nanotubes
P1 - P9	Pores
PM	Powder Metallurgy
PUF	Polyurethane foam
RT	Room Temperature
R^2	Coefficient of determination
SiC	Silicon carbide
SiC_p	Silicon carbide particles
TEM	Transmission Electron Microscopy
TiH_2	Titanium hydride
TR	Transversal Reinforced
TT	Testing Temperature
UR	Unreinforced
W	Energy absorption
W_d	Energy absorption corresponding to densification strain
$W_{50\%}$	Energy absorption corresponding to 50% strain
$W_{50\%,d}$, $W_{50\%,qs}$	Impact and quasi-static energy absorption corresponding to 50% strain
ZrH_2	Zirconium hydride
Δ	Displacement
ε	Strain
ε_d	Densification strain
σ	Stress
σ_d	Stress corresponding to densification strain
σ_{max}	Compressive strength
σ_{pl}	Plateau stress
σ_y	Yield stress
$\sigma_{y,d}$, $\sigma_{y,qs}$	Impact and quasi-static strength
$\sigma_{20\%}$, $\sigma_{40\%}$	Stresses corresponding to 20% and 40% strain

reported that the quasi-static properties of regular MFs increase by 42.91% (σ_{max}), respectively 49.40% (W) with the decrease of TT from 25 to −196 °C. The authors observed the same tendency for the reinforced foams, highlighting an increase of over 44% for both properties. The quasi-static and dynamic properties of closed-cell aluminium foam (ALPORAS) are presented by Cady et al. [30] at different TTs (-196, −100 and 22 °C). They found that σ_{max} exhibit a high dependence on TT, increasing from ~2.0 MPa (22 °C) to 3.6 MPa (-196 °C) – an 80% change. Furthermore, compared to RT, a 70% increase of the W performances of the foam material was obtained when exposed to low TTs. Recently, Fiedler et al [32] investigated the compressive behaviour and mechanical properties of treated and untreated A356 and ZA27 Metallic Syntactic Foams (MSFs) at CT. Their analysis shows a significant embrittlement of MSFs, with a more pronounced effect for the ZA27 matrix. Compared to RT, an initial σ_{max} and W increase of both MSFs was observed at CT. The thermal treatment (applied to increase the matrix ductility) proved no significant improvement of ZA27 foam properties, while a distinct performance enhancement at CT was achieved for A356 foams.

On the other hand, the main physical and mechanical properties under high TTs were reported on regular MFs [33–35], on MSF [36–38], and on reinforced MF [28,35]. Their results show that increasing TTs significantly affect all properties of the foams. These property changes are attributed to the different collapse mechanisms (brittle-to-ductile transition) that take place in the samples with the increase of TT [28,33–38]. The results of Aakash et al. [39] indicates a linear trend of increasing limit/plateau stresses and densification strain of open-cell aluminium foam with the increase of TT (20, 150, 200, 250, and 300 °C). Wang et al [34] observed an increased rate-sensitivity as the TT increases from 25 to 500 °C, while Movahedi et al [40] mentioned a linear degradation of the MFs plateau stress and the W as TT increases (25, 150, 300, and 450 °C). Furthermore, Linul et al [33] investigated the combined effect of temperature (25, 150, 300, and 450 °C) and anisotropy (axial and lateral loading) on the compressive behaviour of cylindrical closed-cell aluminium foams and found that high temperatures highlight a significant degradation effect. The compressive properties of expanded perlite/A356 MSFs were investigated by Taherishargh et al. [38] at different TTs, in the range of 25–500 °C. They observed that the elastic stiffness, σ_{max} and W of MSF samples significantly decrease with increasing TT. In addition, a linear variation of MSFs energy absorption capacity with TT was reported. Yang et al [35] evaluated the high temperature compressive properties and W response of in-situ grown carbon nanotube (CNT) reinforced composite metallic foams (CMFs). The authors observed that both the σ_{max} and W capacity decrease with increasing TT (from 25 to 250 °C), but increase with the increment of CNT content. Also, they found that, at 25 °C, the yield and plateau stresses of CMFs are about 1.6 and 0.8 times higher than that of the pure aluminium foam, respectively

As mentioned by Yang et al [35], Taherishargh et al. [38] Linul et al [28,37], Orbulov et al [41–43] and Katona et al [44,45], the use of various reinforcements for high-strength CMFs are crucial to optimize the crush and energy absorption response of these newly-developed composite structures. The crashworthiness performance and lightweight optimization design of CMFs is based on the research on the best geometric parameters and material configuration to obtain the most appropriate properties during the crushing process. In the literature, to the best of the authors' knowledge, impact properties of lightweight CMFs at high temperatures have not yet been reported. Therefore, this paper investigates the impact compressive response of unreinforced and reinforced metallic foams under extreme thermomechanical conditions (elevated temperatures and different strain-rates). Moreover, the samples collapse mechanisms are discussed together with a microstructural analysis of the foams. In addition, comparisons are made between dynamic and quasi-static data in terms of the strength properties and the absorption energy performances, in the range of 25–350 °C.

2. Materials and methods

2.1. Materials

2.1.1. Aluminium foams

The powder metallurgical (PM) route was used to prepare expanded metal mesh (EMM) reinforced metallic foams. The EMM reinforced metallic foams were prepared in one technological step during the foaming of powder metallurgy (PM) foamable precursor in a mould also containing expanded metal meshes. The foamable precursor was prepared from AlSi10 powder (Mepura GmbH, Austria) mixed with 0.4 wt% of TiH_2 (Titanium hydride) (Chemetall GmbH, Germany) as a foaming

agent. After 30 min of mixing in a Turbula mixer it was cold isostatic pressed at 300 MPa and subsequently hot extruded via direct extrusion at 450 °C. The final PM foamable precursor has almost 100% theoretical density. During foaming of foamable precursor there is no significant reaction inside foam so the final composition is identical with the composition of used powders. Composition data are taken from powder providers and correspond to the precursor composition (see Table 1).

The pieces of foamable precursor were further foamed in computer controlled special foaming equipment, together with expanded metal meshes positioned on the top and at the bottom of the inner space of the mould. The precursor was heated above the melting temperature of used AlSi10 alloy. The EMM reinforced metallic foam was created by cooling the mould down to room temperature after the foam filled the mould. The final size of EMM reinforced metallic foam plates was 500 mm × 500 mm × 30 mm, and the density of foam core of prepared composites was in the range of 400–440 kg/m^3.

2.1.2. Expanded metal mesh (EMM)

Fig. 1 presents the pattern of EMM reinforcement together with the geometrical parameters of the EMM unit-cell (purchased from ITALINOX Slovakia, s.r.o.).

For the experiments, stainless steel X5CrNi 18–10 was used due to considered industrial application of the investigated composite foams in trains. The reason is that this steel is austenitic Cr-Ni stainless steel with corrosion resistance to most oxidizing acids and also salt spray. However, cheaper steel grade EMMs can be used for less corrosive environment. The chemical composition of the EMM is received from the manufacturer and is presented in Table 2. (Table 2).

As was mentioned above, the EMM sheets were inserted into the mould together with foamable precursors. When foam is expanding above the melting temperature of an alloy, the inner pressure inside foam infiltrates molten foam surface skin into the unit cells of EMM reinforcement and even behind it. Further, the reaction between the liquid foam and reinforcement material during foaming takes place. Basically, Si from molten aluminium foam react with Fe and Cr. The thickness of the interface is around 60–80 μm (see Fig. 2). Thanks to this, a strong metallurgical bond is formed between the foam alloy and reinforcements.

Moreover, Simancik et al [46] observed metallurgical bond between EMM and AlSi12 aluminium foam. Using transmission electron microscopy (TEM), the authors identified the Al12Fe3Si interfacial phase between stainless steel and foam. They concluded that this interfacial layer does not represent “the weakest link”; as its properties are usually better than the properties of highly porous and brittle foam matrix. The similar effect can be expected for the investigated composite metallic foams.

2.2. Sample preparation

In order to prevent any damage to the foam cellular structure, an Electric Discharge Machining (EDM) was used for cutting of smaller samples from large foamed plates (Fig. 3a). Therefore, cubic EMM reinforced foam samples (geometry 30 mm × 30 mm × 30 mm), with an average density of 420 kg/m^3 were obtained. The samples with density below or above the 10% range were excluded prior to experiments. The density of the samples was calculated as the ratio between their mass and volume.

Finally, three types of metallic foams were obtained, these being noted as follows: unreinforced (UR), transversal reinforced (TR) and longitudinal reinforced (LR). Fig. 3b and 3c show the detail regarding the loading mode according to the positioning of the EEM reinforcements.

Table 1
Chemical composition of aluminium foam core in composite metal foam.

Si [wt. %]	Ti [wt. %]	Fe [wt. %]	Al [wt. %]
10	0.4	0.1	Bal.

2.3. Experimental setup

The experimental program was designed to investigate the impact and quasi-static compressive properties of EMM reinforced metallic foams at five different testing temperatures (TTs), i.e. 25 °C, 75 °C, 150 °C, 250 °C and 350 °C. The compression tests were performed in an automatically controllable thermal chamber with a standard deviation of ± 3 °C from each TT. In order to ensure a thermal equilibrium and to obtain a homogeneous distribution of temperature throughout the mass of the samples, before the impact and quasi-static tests, the samples were kept in the thermal chamber for 20 min at desired TT. Moreover, to prevent the temperature reduction after preheating, all samples were tested inside the thermal chamber. The tests were performed and main properties determined according to the ISO 13314-11 standard [47].

2.3.1. Impact tests

The impact crashworthiness performances of unreinforced (UR) and reinforced (LR and TR) foams were investigated by using an Instron Dynatup instrumented drop tower system, equipped with a thermal chamber. The used testing machine was equipped with data acquisition software and a maximum 45 kN force transducer. A compression strain rate of 95 s^{-1} was adopted to ensure that all samples have a deformation of over 80%. This strain rate gave an initial velocity equal to 2.8 m/s. In order to obtain the desired velocity and the deformation of the samples, a hammer with the mass of 5 kg was used.

2.3.2. Quasi-static tests

The identical experimental procedure (testing temperatures, shape and size of samples, loading directions) was adopted for the quasi-static mechanical characterization of the obtained samples. After a preload of 0.01 kN was applied to remove any surface irregularities, compressive loading was applied quasi-statically using displacement control at a constant nominal crosshead speed of 10 mm/min (0.17·10^{-3} m/s). Uniaxial compression tests were carried out on a 100 kN LBG TC100 electromechanical computerized universal testing machine, equipped with a thermal chamber. The quasi-static results were used for the impact-static comparative study.

2.4. Microstructure analysis

The microstructural analysis was used to identify the type, size and shape of the foam cell structure. In addition, investigations were carried out regarding the deformation modes of the unreinforced and reinforced foams at different testing temperatures. For this purpose, an Insize ISM-M1000 metallurgical inverted microscope was used. In order to be morphologically characterized by SEM imaging, the tested foam samples were first cut in half using a water jet-cutting machine. Then, the cut samples were embedded in self-curing acrylic resin (Duracryl Plus), followed by their polishing until a mirror gloss surface was obtained. Further, to obtain a finer surface, abrasive discs with different granulations (320, 600 and 1200) were used successively. Finally, a felt disc with a colloidal alumina suspension of 0.05 μm was used, leading to the final surface to be analyzed.

3. Results and discussions

3.1. Impact behaviour

Load (F) - displacement (Δ) curves were collected during the experimental tests by the software linked to the testing machine and were converted into stress ($\sigma = F/A$) and strain ($\varepsilon = \Delta/l_0$) using sample dimensions; where F and Δ are the load/displacement measured by the compression-tension load-cell, l_0 is the initial high and A is the effective

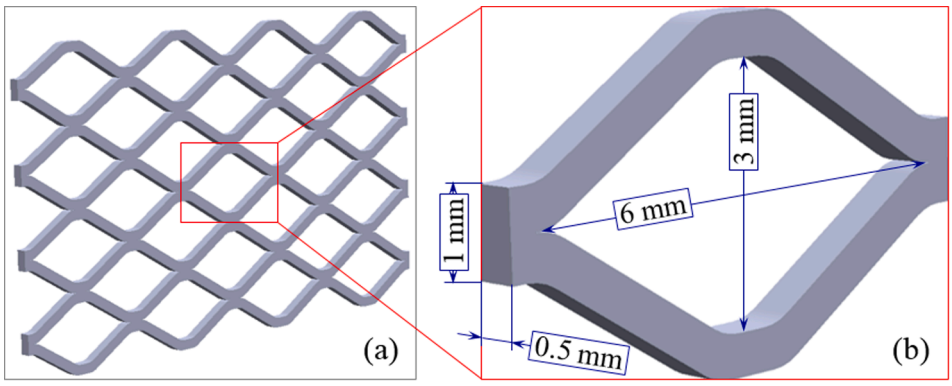

Fig. 1. Pattern (a) and unit-cell dimensions (b) of the EMM reinforcement.

Table 2
Chemical composition of EMM steel X5CrNi 18–10.

Cr [wt. %]	Ni [wt. %]	C [wt. %]	Si [wt. %]	Mn [wt. %]	Fe [wt. %]
17–19.5	8–10.5	<0.07	<1.0	<2.0	Bal.

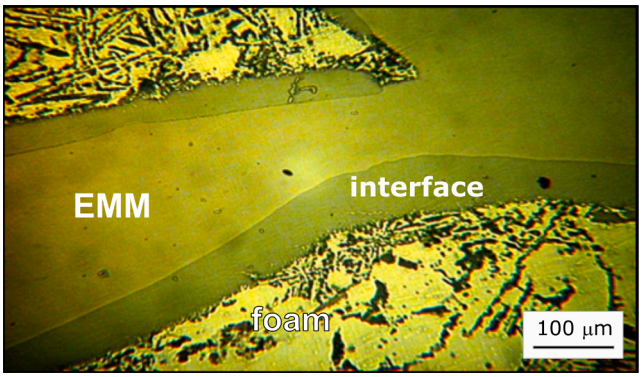

Fig. 2. The interface between stainless steel X5CrNi 18–10 and AlSi10 foam.

cross-sectional area of the samples. A similar pattern of stress–strain behaviour can be observed between UR (Fig. 4a), TR (Fig. 4b) and LR (Fig. 4c) metallic foams as the TT rises.

This F-Δ → σ-ε conversion provided a typical compression behaviour, being similar to most cellular materials [47,48]. From Fig. 4, the compression behaviour of both reinforced and unreinforced metallic foams exhibits three characteristic regions: linear-elastic, plateau and densification region. The effective stiffness of the foam is obtained from the slope of the first linear elastic region, while the foam compressive strength (σ_{max}) is given by the end of the first region where the first maximum in the stress–strain curve is identified. Previous investigations of closed-cell metallic foams [49,50] have found that the linear-elastic response is related to the face stretching and edge bending in closed-cell foams. It can be observed that all σ-ε curves show a maximum visible and easily identifiable point. In the case of cellular materials (metallic, polymeric and glass foams), this compressive strength is associated with the yield stress (σ_y). As the stress gradually increases, the foam cells begin to collapse by yielding, elastic buckling, bending and fracture. Of course, depending on the test conditions and foam type, these failure mechanisms occur individually or in groups. After the yield point, the investigated foams have a long plateau region, from which the plateau stress (σ_{pl}) is determined. The initial stress drop between the elastic and the plateau regions is marked by the appearance of the first deformation band in the sample [51]. The σ_{pl} is determined as the arithmetic mean between the stresses corresponding to deformations of 20%, respectively 40% strain (more precisely $\sigma_{20\%}$ and $\sigma_{40\%}$). The shape and size of the plateau area can be controlled by the collapse mechanisms that occur during compression tests (e.g. yielding/buckling/bending/fracture of cell walls), by the type of foam (reinforced/unreinforced foams, closed/open cell foams, etc.) and by the test conditions (low/room/high temperature, impact/quasi-static tests, etc.). In this case, the dominant deformation mechanisms that affected the shape of the σ-ε curves were governed by the impact loading condition and the testing temperature. The σ-ε curves had relatively large oscillations considering the type of the foam and testing temperature. These oscillations are associated with the more brittle nature of the AlSi10 matrix under impact loads, the appearance of the inertia effect and the progressive development of the already formed deformation band [52,53]. The plateau region is very important for the engineering materials used in energy absorption applications, especially impact applications. In fact, because this region spans over 80% of the entire σ-ε curve, the absorption energy (W), which is represented by the area underneath the curve, is high. Finally, the end of the plateau region is preceded by the onset strain of densification. The identification of this point, common to the two regions, leads to the determination of the main specific properties of the onset strain of densification, namely densification strain (ε_d), stress corresponding to densification strain (σ_d) and absorption energy corresponding to densification strain (W_d). The steeper slope of the σ-ε curve within the densification region is defined as the foam densification modulus. In this region the cell walls come into contact

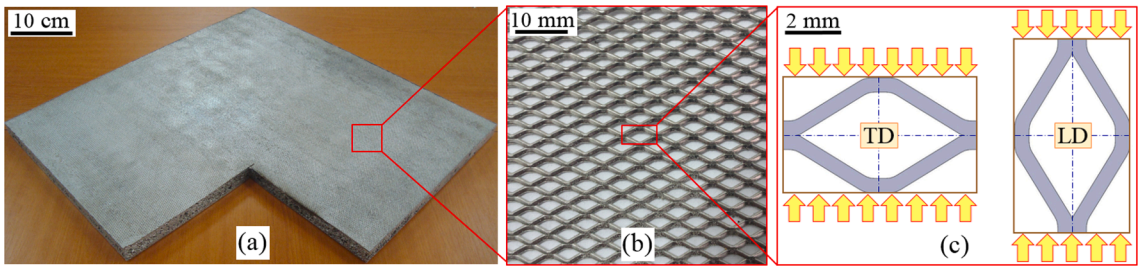

Fig. 3. Foam panel (a), EMM reinforcement (b) and unit-cell orientation (c), according to loading direction.

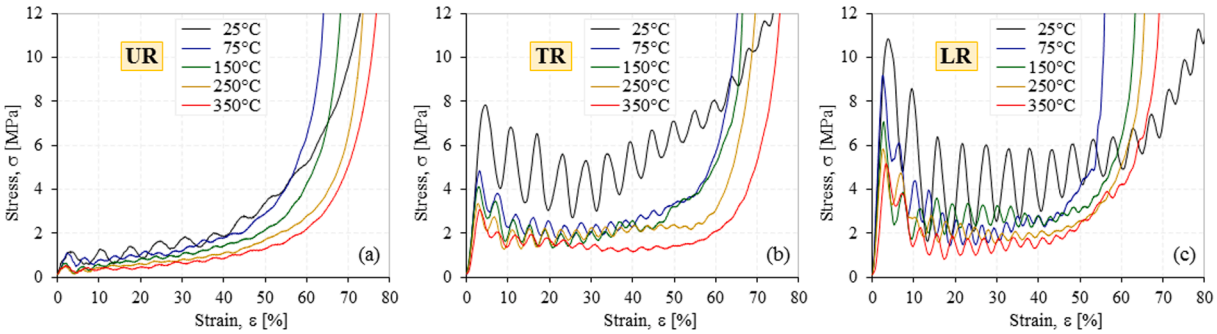

Fig. 4. Influence of TT on σ - ε curves of UR (a), TR (b) and LR (c) metallic foams (strain rate 95 s^{-1}).

with each other, and the foam begins to behave as a solid material (the solid material from which the foam is made).

From Fig. 4 it can be observed that, regardless of the type of tested foam (UR, TR or LR foam), the intensity of the oscillations significantly decreases with increasing testing temperature. The same phenomenon is observed in the case of the compression behaviour, whereby the main mechanical properties of the foams decrease with the increase of temperature. This is because the elastic, strength and energy absorption properties are directly linked to the magnitude of the global stress–strain curves, according to the nature of the test. Moreover, besides the testing temperature, it was observed that the use of reinforcements completely changes the main properties of investigated foams. By using expanded metal mesh (EMM) as a reinforcement, an improvement in the compression behaviour of the foams is obtained. In addition, the longitudinal positioning of the reinforcements (LR) seems to have much better capabilities to withstand the impact loads, at the same weight of samples.

3.2. Impact properties

In order to describe the analysis and comprehension of the experimental results obtained for UR, TR and LR foams, a comparison of strength properties (σ_y, σ_{pl} and σ_d) and energy absorption performances (W_d) determined according to ISO 13314–11 Standard [47] was performed (see Fig. 5). It was observed that the obtained properties monotonically decreases with an increase in TT, and this relationship is nearly identical for all properties. This phenomenon is associated with the softening of the cellular structure of the foam with the brittle-to-ductile transition.

The results from Fig. 5a show that, compared to unreinforced foams, the use of EMM reinforcements increased the compression strength ($\sigma_{max} = \sigma_y$) of LR foams by 5.88 times and up to 8.50 times for LR foams. This difference in terms of σ_{max} remains almost constant for all temperatures. In terms of the two types of reinforcements, LR foams highlights higher compressive strength than corresponding TR foams at all investigated temperatures. This difference increases approximately linearly with increasing TT from 30.75% (at 25 °C) to 40.34% (at 350 °C). Between 25 and 150 °C, the plateau (σ_{pl}) and densification (σ_d) stresses exhibit the same pattern, having the maximum value represented by the TR foam, followed in order by LR foam and UR foams respectively (Fig. 5b and c). At test temperatures higher than 150 °C, LR foam shows better σ_{pl} than TR and UR foams, while the σ_d is higher in the case of UR foams. In the case of room temperature (25 °C), the σ_{pl} is higher by up to 2.59% in favour of reinforced foams, this difference decreasing up to 1.75% at 350 °C. On the other hand, all foams have values quite close in terms of σ_d.

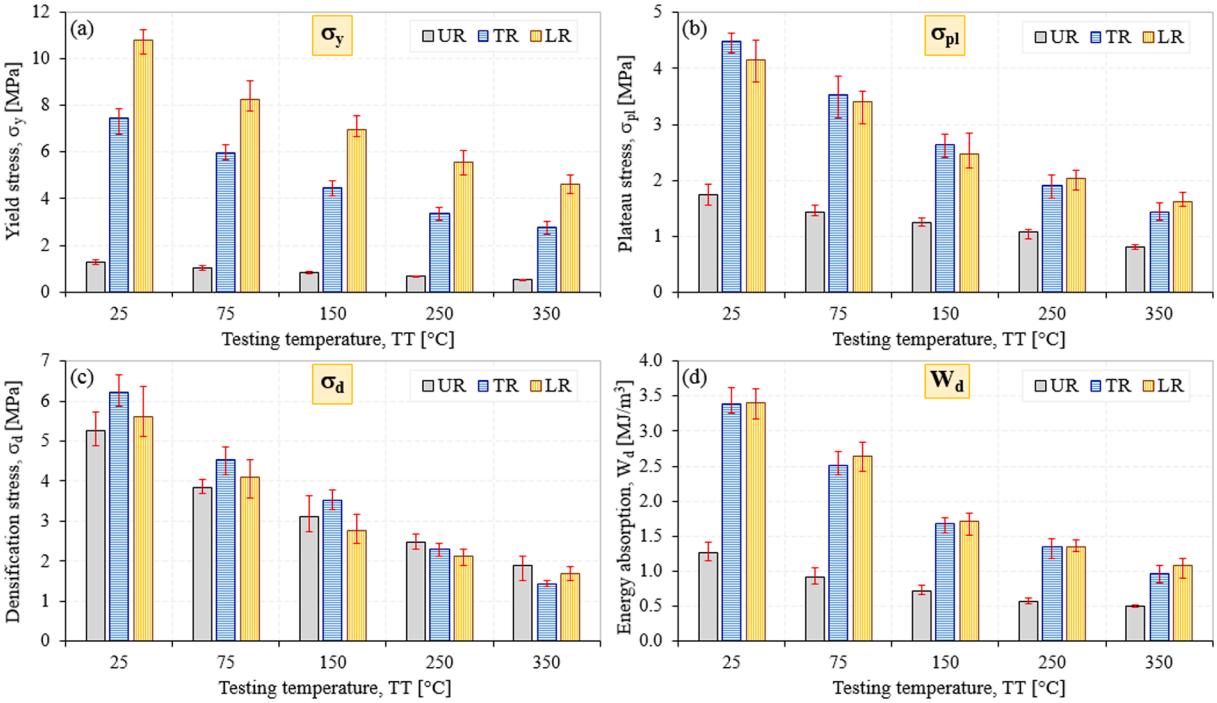

Fig. 5. Variation of yield (a), plateau (b), densification (c) stress and energy absorption (d) with TT (strain rate 95 s^{-1}).

Fig. 5d shows the compressive results for the energy absorption performances at densification strain (W_d). As is obvious from this figure, the least value of the W_d was 1.26 MJ/m^3 belonging to the UR foam at 25 °C, with a polynomial decrease between 27.22% (75 °C) and 60.12% (350 °C) with respect to the TT. The largest W_d value was 3.39 MJ/m^3 belonging to the both TR and LR foams at the same TT (25 °C), which was 62.83% higher than that of unreinforced foam. At all other temperatures (75–350 °C), TR foams showed better W_d properties than LR foams, while the properties of UR foams were up to 65% lower than for the other two reinforced foams. The foam samples having a transversal reinforcement exhibited a better plastic dissipation of the impact energy. The maximum energy capacity of the Instron Dynatup instrumented drop tower system is 300 J, energy developed for a maximum velocity of 5 m/s. Taking into account the fact that the experimental tests were performed with a velocity of 2.8 m/s, the maximum energy developed by the machine is approximately equal to 160 J. In this case, the total energy absorbed by the samples is around 150 J. Of course, as previously mentioned, the amount of this energy depends on the test temperature and the positioning of the reinforcements. The experimental tests showed that the foams with reinforcements had a more homogeneous collapse in the transversal loading direction. Therefore, during the manufacturing process, the orientation of EMM reinforcements on structural elements is important, in order to provide the best operating safety conditions. Regarding the standard deviations of the results that appear after the compression tests, it can be observed that the LR foams present higher errors than the UR and TR foams. This phenomenon can be associated with much greater distance between two consecutive cells of the EMM reinforcement (large diagonal of the rhombus), which leads to the unstable deformation of the reinforcement cell (see Fig. 1).

The reduction of the properties for investigated samples at different TTs was further analysed. For the proper display of this evolution, the two strength properties (σ_y and σ_{pl}) and the energy absorption performance (W_d) were normalized with respect to room temperature values. Fig. 6 compares the percentage reduction of the normalized compressive strength (Fig. 6a), plateau stress (Fig. 6b) and energy absorption capabilities (Fig. 6c) for UR, TR and LR foam samples.

All three properties show almost the same tendency and are thus discussed together [38]. Up to 75 °C there is a large percentage reduction of all properties, except the W_d which has this pronounced reduction up to 150 °C. Beyond these values (75 °C for σ_y and σ_{pl}, and 150 °C for W_d), the percentage reduction of the properties is in a continuous linear growth, but not as pronounced as before. A similar relative σ_y reduction is observed for UR and LR foams, while TR samples shows higher reduction of up to 12%. The σ_{pl} and W_d reduction of the unreinforced foam is considerably below the reduction percentage of the reinforced samples (see Fig. 6b and Fig. 5c). As shown in Fig. 6b, the highest percentage reduction and at the same time the degradation of the σ_{pl} is obtained for the TR foam. The W_d property reduction of the LR foam samples is only slightly below the TR sample (Fig. 6c).

3.3. Microstructural analysis

All the investigated samples displayed good progressive deformation mechanisms. The mechanical performances of MFs are governed by their geometrical features, of which the most important are apparent density (low, medium or high density), manufacturing defects in the cell structure (micro-cracks, intracellular cavities, micro-pores, etc.), distribution in cell size, cell shape and size, as well as the microstructural parameters (cell-wall thickness, material distribution between cell-wall and cell-edge, edge geometry) [33,40,54,55]. The three specific regions (linear-elastic, plateau and densification), mentioned in Section 3.1, highlights different mechanisms of deformation. In the linear-elastic region, the strain concentrations are not obvious, only local plastic deformations of the cell walls are observed. Further, during plateau region, plastic buckling, bending and fracture of the cell walls in weaker cells (curved cell walls, cracked cell walls or elongated cells) leads to local stress concentrations in neighbouring cells and finally the appearance of deformation bands. Once these bands are formed within the densification region, their successive collapse occurs, finally leading to the densification of the foam cellular structure. Of course, depending on the testing temperature, these collapse mechanisms differ significantly. Fig. 7 presents a stereographic view of the MF samples obtained after compression tests. The figure shows details of the collapse mechanisms for each investigated temperature.

In order to be able to be compared, all the samples are tested up to the same applied load, and the images are collected to the same magnification (10×). The UR foam samples exhibit the highest densification of structure, then TR foams, finally LR foams are less dense at all TT. All three types of foams, whether they are reinforced or not, present the same failure mechanism at a certain temperature, and are thus discussed together. At room temperature (25 °C), the solid material from which the foams are made, have a brittle matrix (BM). Due to the high brittleness of the matrix, many micro-cracks are initiated and later propagated in the foam structure, resulting in the appearance of a brittle fracture mechanism. As can be seen in Fig. 7, the fracture of the cell walls is brittle, without any remaining plastic deformation (see yellow ellipses with dashed lines at 25 °C). Increasing the TT to 75 °C, it is observed that the foam matrix begins to slowly lose its brittleness. Because the temperature is not very high, most cell walls collapse by brittle fracture (yellow ellipses at 75 °C). However, it can be seen that between certain neighbouring pores (P1 ↔ P2, P2 ↔ P3, P4 ↔ P5, P4 ↔ P6, P7 ↔ P8 and P8 ↔ P9), where the cells have very thin walls, there is a plastic buckling of the walls (see the green arrows at 75 °C). As the TT rises to 150 °C, the matrix begins to soften more and more, while brittle failure occurs only in isolated areas. Instead, it is replaced by a pronounced plastic deformation of the cell walls (see the red curved lines at

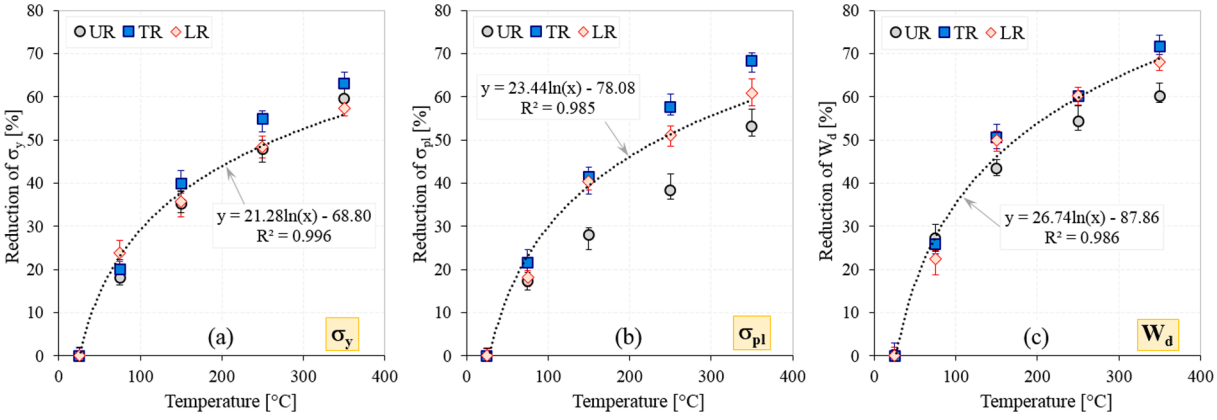

Fig. 6. Reduction percentage of σ_y, σ_{pl} and W_d at different TT normalized by RT value (strain rate 95 s^{-1}).

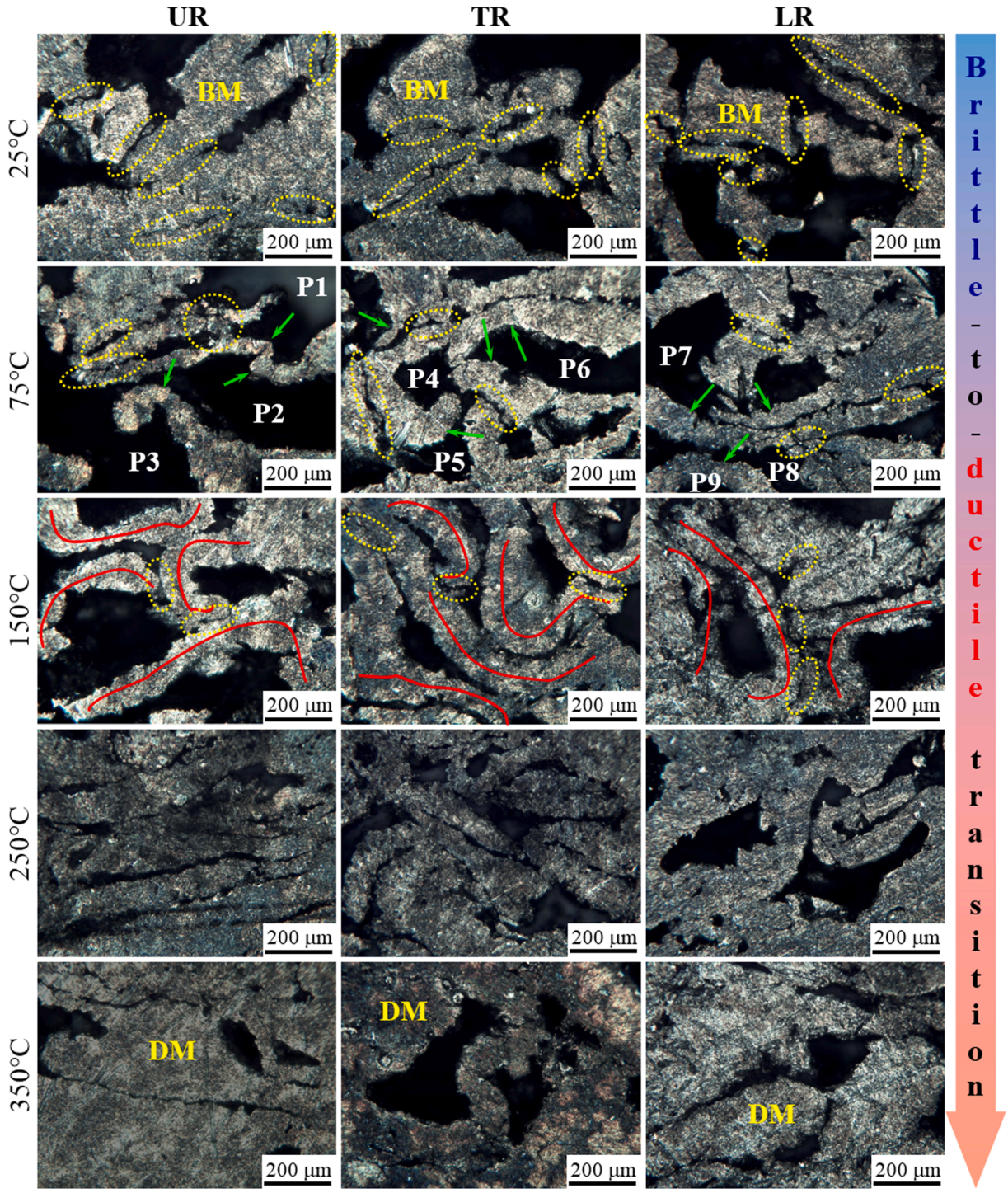

Fig. 7. Stereographic view (10 × magnification) of impact deformation process under different TTs tested up to the same applied load.

150 °C). Finally, increasing the TT to 250 °C and then further to 350 °C, it is observed that foam exhibit a ductile matrix (DM). Due to the dynamic recrystallization process and softening of the matrix material, the cell walls begin to come into contact with each other, and a brittle-to-ductile transition takes place [56]. In this case, in contrast to 25 °C, only a high degree of plastic deformation is highlighted, without the appearance of brittle fracture.

4. Comparison between impact and quasi-static results

This work also presents a detailed comparison of the impact results with data obtained under quasi-static loading conditions. The experimental program followed the same procedure for both types of tests.

4.1. Compressive behaviour

Fig. 8 illustrates a comparison of impact and quasi-static compressive stress–strain curves of investigated metallic foams at room temperature. Comparisons were made at all temperatures used for impact tests (25, 75, 150, 250 and 350 °C), but in order to avoid repeating the graphs, only curves at 25 °C were presented, as the other temperatures followed the same trend.

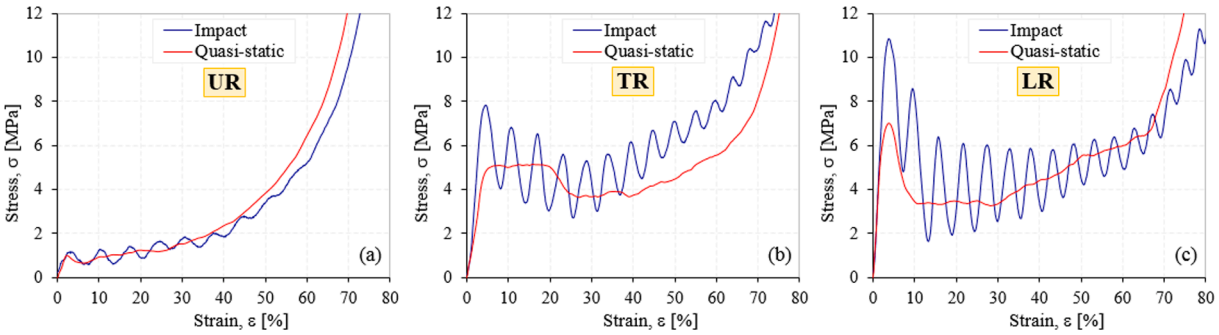

Fig. 8. Impact (strain rate 95 s^{-1}) and quasi-static (strain rate $5.77 \cdot 10^{-3}$ s^{-1}) σ - ε curves of UR (a), TR (b) and LR (c) metallic foams at 25 °C.

The two types of tests show very different behaviours regarding the σ - ε curves. It can be seen that impact behaviour has excellent compressive strength characteristics (higher load curves, especially for the yield point), while quasi-static behaviour highlights good and more stable failure patterns (smaller stress fluctuation ranges). In the case of quasi-static tests, due to the lack of large oscillations, both the plateau region and the onset strain of densification are more obvious. Generally, under impact conditions, the matrix material behaves more brittle compared to quasi-static due to the sudden change of the collapse mechanisms. Excluding the UR foam, it is observed that the densification strain presents higher values in the case of quasi-static tests, the length of the plateau also being larger. Moreover, the plastic deformation mechanisms and the crushing performance of the reinforced foams occur at higher compressive stress levels compared to the unreinforced foams.

4.2. Assessment of properties

In order to be able to interpret more precisely the properties obtained from the two tests, Fig. 9 shows a comparison of the compressive strength and the energy absorption capacity according to the testing temperature and the type of foam sample. To have the most conclusive results, the compressive strength (σ_{max}) was associated with the first peak stress after the linear-elastic region of the stress–strain curve, while the absorption energy ($W_{50\%}$) was calculated up to 50% strain for all samples according to ISO 13314–11 standard [47], using the Eq. (1).

$$W_{50\%} = \int_0^{50\%} \sigma d\varepsilon \tag{1}$$

Fig. 9a–c present measured compressive strength values of UR, TR and LR samples, obtained by impact and quasi-static compression tests. These values decrease with increasing TT and were averaged over five test results. It was observed that the impact compressive strength of the foam samples showed a polynomial relationship as a function of TT, while under quasi-static conditions the σ_{max} reveal an almost linear decrease. The impact tests exhibit a higher compressive strength than that of the quasi-static tests when subjected to the same TT. The largest impact – quasi-static σ_{max} difference – is found at room temperature (24.90% for UR, 35.79% for LR and 37.26% for TR), followed by a slight decrease for 75 °C (14.88% for UR, 18.04% for LR and 29.07% for TR). With the increase of TT, the compressive strengths of the two tests are getting closer and closer, showing differences of only 3% at 350 °C.

Conversely, it was found that the absorption energy (area under the σ-ε curves up to 50% strain) in the case of quasi-static tests is significantly higher than in the case of the impact tests. This phenomenon can be associated with the more stable deformation mode during quasi-static tests, highlighted by the shape of the σ-ε curves due to the lack of oscillations, by the size of the plateau region and by the delayed onset strain of densification. Regardless of the type of foam (UR, TR or LR foam), as the temperature increases (25 °C → 350 °C), the absorption

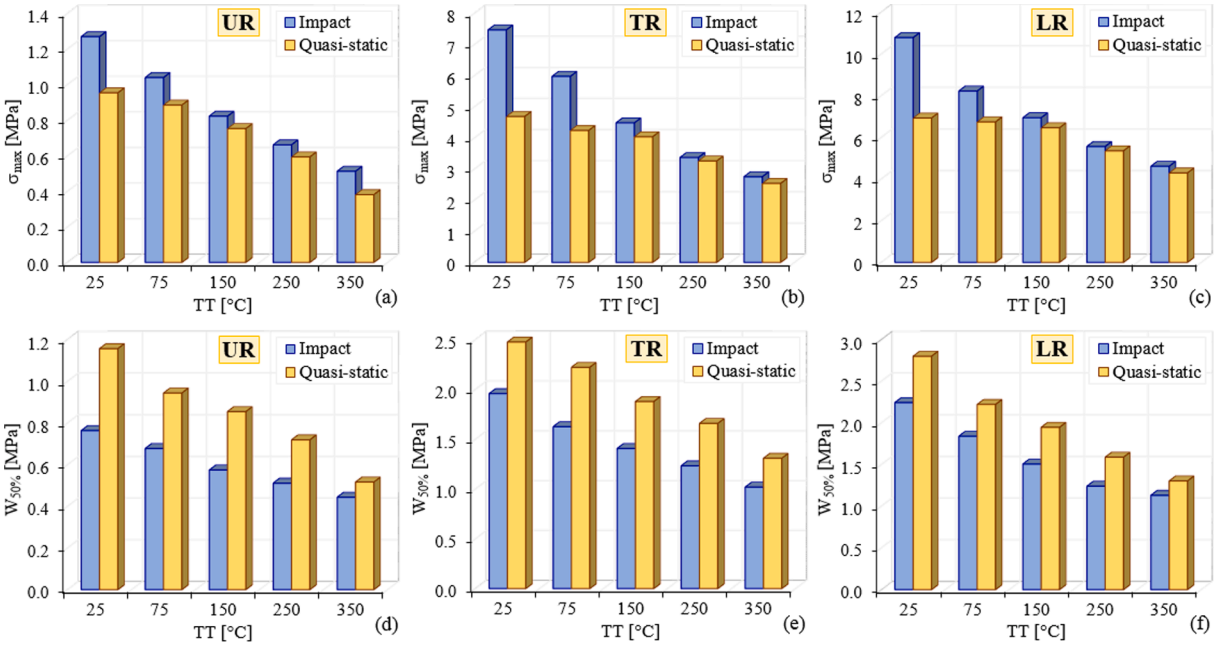

Fig. 9. Comparison of impact and quasi-static properties (compressive strength and energy absorption) according to TT.

energy decreases polynomial for impact tests and linear for quasi-static tests, respectively. As in the case of compressive strength, the biggest $W_{50\%}$ difference, in detriment of impact tests, is obtained at 25 °C (51.47% for unreinforced foams and about 25% for EMM reinforced foams). Compared with the strength property (σ_{max}), in case of energy absorption performances ($W_{50\%}$), these differences are somewhat significant even at high temperatures (over 15% at 350 °C).

Fig. 10 shows a variation of the main impact properties (i.e. compression strength and energy absorption) depending on the quasi-static ones.

The impact compression strength varies polynomially with the quasi-static one (Fig. 10a–c), while the energy absorption varies according to a linear function (Fig. 10d–f). Based on the quasi-static experimental results, empirical formulae are proposed to predict the impact properties of newly-developed CMFs (see the equations in the graphs). All these equations show a very good coefficient of determination (R^2), higher than 0.98 for all the presented cases. The proposed equations are very important for practical applications, because determining the impact properties at high temperatures is quite difficult to achieve. In addition, the experimental set-up in dynamic regime is expensive and requires special equipment. Therefore, using these equations the impact properties of the CMFs can be determined if the quasi-static ones are known, the latter ones being determined relatively easily compared to the impact properties.

As previously mentioned (see Introduction section), many researchers have studied the effect of reinforcement and strain rate on the main mechanical properties of aluminium alloy foams, but mostly at room temperature [25,57,59]. Some have reported contradictory effects of these factors on the compressive behaviour of their developed CMFs. For example, Sahu et al. [25], using 10 wt% silicon carbide particles (SiC_p) as reinforcement and AA2014 aluminium alloy as matrix material, reported, at 25C, a value of only 34% for densification strain, almost half than TR foams. Moreover, they obtained a yield stress 2.83 times lower compared to LR composite foams. Yadav et al [57,58] observed that CMFs reinforced with 10 wt% Silicon carbide (SiC) particles are superior to those reinforced by 1.5 wt% multi-wall carbon nanotubes (MWCNTs). Even so, their energy absorption values are up to 24% lower than EMM-CMFs [57]. However, due to the different collapse mechanisms, Yadav et al [58] obtained values for the plateau stress up to 60% higher than the CMFs reported in this investigation. Furthermore, increasing the temperature from 25 to 400C, they have achieved a decrease of about 30% of the plateau stress for the two types of CMFs, twice as small as EMM-CMFs. Birla et al. [59] studied the effect of relative density and cenosphere particle size on the compressive mechanical behaviour of aluminium-cenosphere composite foams. They obtained values of plateau stress and energy absorption performance similar to those reported by Yadav et al [57] for CMFs reinforced with 10 wt% SiC particles. However, all these differences are mainly due to different strain rates (0.01 [25,57,59], 1 [58] and 95), the type of reinforcement (SiC_p particles [25], SiC particles [57,58], MWCNTs [57,58], cenosphere [59] and EMM), reinforcement size (20 to 40 μm [25], 30 μm 57], 50 μm [58], 50 nm × 25 μm [57], 5.1 mm [59] and 3 mm × 6 mm), matrix material (AA2014 [25], AlSi12Cu1Mg1 [57–59], AlSi10) and foaming agent (ZrH_2 [25], CaH_2 [57,59] and TiH_2 [58]). The results are provided for the same relative density (0.16) and the same test temperature (25C), respectively.

Additionally, the relative reduction percentage of the impact and quasi-static properties for both unreinforced and reinforced foams were compared. The results are normalized by room temperature value, and presented according to the TT. Fig. 11 presents the reduction percentage of σ_{max} values as a function of TT between the impact and quasi-static tests (circular and square blue markers). In the range of 75–350 °C, the observed σ_{max} trendline is quite similar between the two test conditions. Even if the results show the same tendency, however, it can be

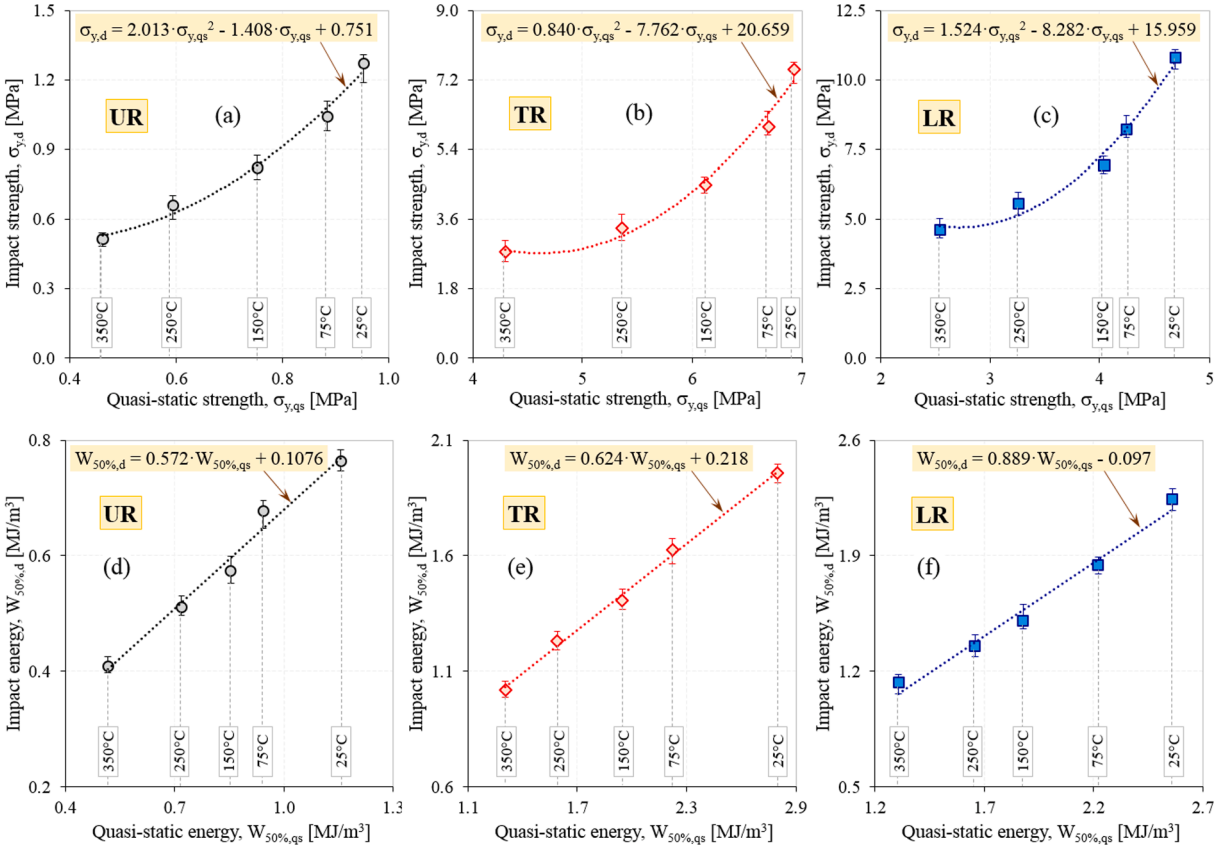

Fig. 10. Variation of the impact properties ($\sigma_{y,d}$, $W_{50\%,d}$) depending on the quasi-static ($\sigma_{y,qs}$, $W_{50\%,qs}$).

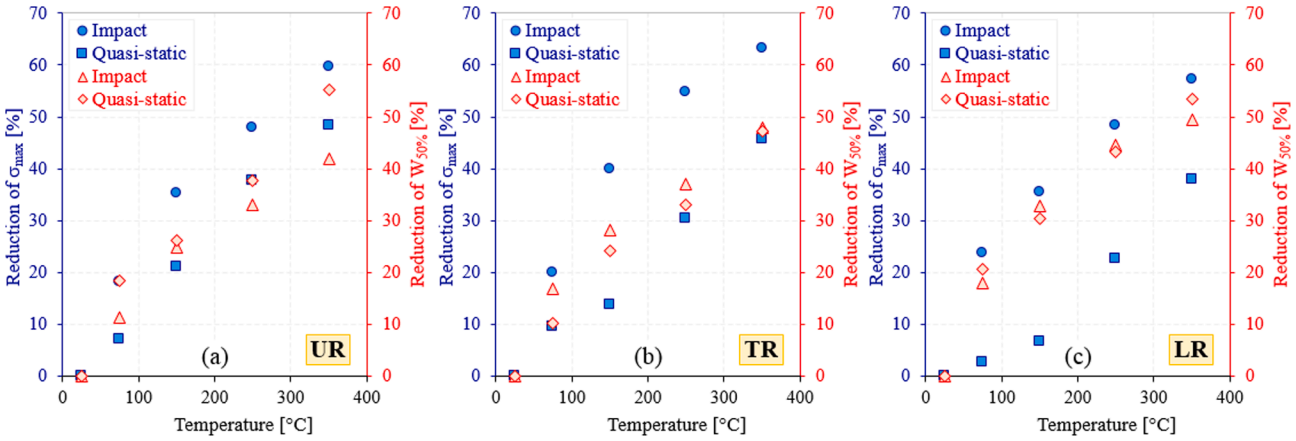

Fig. 11. Reduction percentage of impact and quasi-static properties (compressive strength and energy absorption) at different TT normalized by RT value.

easily observed that the percentage reduction in impact tests is much higher than in quasi-static tests. The biggest difference between the two types of tests (of 8.78 times) is found at 75 °C for reinforced samples (LR foams), decreasing to 2.52 times for unreinforced ones. With the increase of TT, these differences reduce significantly, being only 1.51 times for LR foams and 1.23 times for UR foams at 350 °C.

Related to the reduction of $W_{50\%}$, the observation was made of a slightly larger percentage discrepancy between impact and quasi-static results, which are attributed to the oscillations of the plateau region. The percentage results in terms of $W_{50\%}$-TT variation are compared in Fig. 11 (triangular and rhombic red markers). Energy absorption shows very close percentage reductions for both types of tests. However, compared to quasi-static data, the $W_{50\%}$ reduction in the case of impact tests is higher for the reinforced foams, whereby respectively smaller for the unreinforced ones.

5. Conclusions

The impact compressive response of Composite Metallic Foams (CMFs) as a function of testing temperature (i.e. 25, 75, 150, 250 and 350 °C) was experimentally investigated. The transversal (TR) and longitudinal (LR) reinforced CMFs were compared with unreinforced (UR) ones. Finally, the impact properties (compressive strength and energy absorption) were compared with the quasi-static results. The obtained results leads to the following conclusions:

- Regardless of the type of tested foam (UR, TR or LR foam), the intensity of the oscillations in the plateau region of the stress–strain curves significantly decrease with the increase of the test temperature (TT) phenomenon associated with the foam matrix softening process.
- Due to Expanded Metal Mesh (EMM) anisotropy, the LR samples demonstrate much better capabilities of withstanding compressive loads than TR and UR samples.
- Due to the positioning of the reinforcement, the TR samples collapsed more homogeneously than LR ones.
- Dynamic recrystallization process, together with softening of matrix material, leads to a brittle-to-ductile transition with increasing TT.
- The strength properties and energy absorption performances monotonically decrease with increasing TT in a nearly identical manner.
- The impact tests exhibit a higher compressive strength than quasi-static tests at the same TT. As the TT increases, the compressive strengths of both tests become closer, showing only a 3% difference at 350 °C.
- The percentage reduction of normalized compressive strength in impact tests is much higher than in quasi-static tests.
- The quasi-static energy absorption is significantly higher than in the case of impact tests. This aspect is due to the more stable deformation mode (the lack of oscillations, the size of the plateau region and the delayed onset strain of densification) in quasi-static tests.
- Empirical formulae are proposed to predict the impact properties (compression strength and energy absorption) of new-developed CMFs.

The obtained results are significant for the design of CMFs reinforced with EMMs. They will be used for the design of CMFs as heat exchangers covering the entire pitched roof of a building (project APVV-17–0580). The CMF heat exchangers will not only provide better recovery of the heat, but also dissipate unwanted excess heat from inside when needed. The results of the paper are important for the strength and energy absorption parameters of the development of CMF roof panels.

6. Data availability

The raw data required to reproduce the findings of this work cannot be shared at this time as the data also forms part of an ongoing study.

CRediT authorship contribution statement

Emanoil Linul: Conceptualization, Investigation, Writing - original draft, Writing - review & editing. **Daniel Pietras:** Investigation, Formal analysis, Writing - review & editing. **Tomasz Sadowski:** Funding acquisition, Resources, Software, Writing - review & editing. **Liviu Marşavina:** Funding acquisition, Resources, Writing - review & editing. **Dipen Kumar Rajak:** Investigation, Writing - review & editing. **Jaroslav Kovacik:** Funding acquisition, Resources, Writing - review & editing.

Declaration of Competing Interest

The authors declare that they have no known competing financial interests or personal relationships that could have appeared to influence the work reported in this paper.

Acknowledgement

The financial support by: (1) the Slovak Research and Development Agency under the contract APVV-17-0580 (“Research of roofing with integrated function of heat exchanger”), (2) Ministry of Science and Higher Education (Poland – contract FN 20/ILT/2020) and (3)

Romanian Ministry of Research and Innovation (project number PN-III-P1-1.2-PCCDI-2017-0391) are gratefully acknowledged.

References

[1] Maiorano LP, Molina JM. Guiding heat in active thermal management: One-pot incorporation of interfacial nano-engineered aluminium/diamond composites into aluminium foams. Compos Part A 2020;133:105859.
[2] Nikbakht S, Kamarian S, Shakeri M. A review on optimization of composite structures Part II: Functionally graded materials. Compos Struct 2019;214:83–102.
[3] Rajak DK, Mahajan NN, Linul E. Crashworthiness performance and microstructural characteristics of foam-filled thin-walled tubes under diverse strain rate. J Alloy Compd 2019;775:675–89.
[4] Ashby MF, Evans A, Fleck NA, et al. Metal Foams: A Design Guide. USA: Butterworth-Heinemann; 2000.
[5] Kovácik J, Jerz J, Mináriková N, et al. Scaling of compression strength in disordered solids: metallic foams. Frattura ed Integrita Strutturale 2016;36:55–62.
[6] Li TT, Wang H, Huang SY, et al. Bioinspired foam composites resembling pomelo peel: structural design and compressive, bursting and cushioning properties. Compos Part B-Eng 2019;172:290–8.
[7] Zhou T, Zhang P, Xiao W, et al. Experimental investigation on the performance of PVC foam core sandwich panels under air blast loading. Compos Struct 2019;226:111081.
[8] Xu Z, Duan L, Hou Y, et al. The influence of carbon-encapsulated transition metal oxide microparticles on reducing toxic gases release and smoke suppression of rigid polyurethane foam composites. Compos Part A 2020;131:105815.
[9] Voiconi T, Linul E, Marsavina L, et al. Determination of flexural properties of rigid PUR foams using digital image correlation. Solid State Phenom 2014;216:116–21.
[10] Chen JH, Liu PS, Sun JX. Sound absorption performance of a lightweight ceramic foam. Ceram Int 2020;46(14):22699–708.
[11] Shahapurkar K, Garcia CD, Doddamani M, et al. Compressive behaviour of cenosphere/epoxy syntactic foams in arctic conditions. Compos Part B-Eng 2018;135:253–62.
[12] Pietras D, Linul E, Sadowski T, Rusinek A. Out-of-plane crushing response of aluminium honeycombs in-situ filled with graphene-reinforced polyurethane foam. Compos Struct 2020;249:112548.
[13] Wang E, Sun G, Zheng G, Li Q. Characterization of initial and subsequent yield behaviours of closed-cell aluminium foams under multiaxial loadings. Compos Part B-Eng 2020;202:108247.
[14] Sun G, Wang Z, Yu H, et al. Experimental and numerical investigation into the crashworthiness of metal-foam-composite hybrid structures. Compos Struct 2019;209:535–47.
[15] Wang H, Zhu DF, Hou S, et al. Cellular structure and energy absorption of AlCu alloy foams fabricated via a two-step foaming method. Mater Des 2020;196:109090.
[16] Epasto G, Distefano F, Gu L, et al. Design and optimization of Metallic Foam Shell protective device against flying ballast impact damage in railway axles. Mater Des 2020;196:109120.
[17] Huo X, Sun G, Zhang H, et al. Experimental study on low-velocity impact responses and residual properties of composite sandwiches with metallic foam core. Compos Struct 2019;223:110835.
[18] Movahedi N, Murch GE, Belova IV, Fiedler T. Functionally graded metal syntactic foam: Fabrication and mechanical properties. Mater Des 2019;168:107652.
[19] Liu H, Ding S, Ng BF. Impact response and energy absorption of functionally graded foam under temperature gradient environment. Compos Part B-Eng 2019;172:516–32.
[20] Linul E, Marsavina L, Kovacik J, Sadowski T. Dynamic and quasi-static compression tests of closed-cell aluminium alloy foams. Proc Romanian Acad – Ser A 2017;18(4):361–9.
[21] Zhang J, Chen L, Wu H, et al. Experimental and mesoscopic investigation of double-layer aluminium foam under impact loading. Compos Struct 2020;241:110859.
[22] Wejrzanowski T, Cwieka K, Skibinski J, et al. Metallic foam supported electrodes for molten carbonate fuel cells. Mater Des 2020;193:108864.
[23] Zhang Y, He SY, Liu JG, et al. Density gradient tailoring of aluminium foam-filled tube. Compos Struct 2019;220:451–9.
[24] Kovacik J, Marsavina L, Linul E. Poisson's ratio of closed-cell aluminium foams. Materials 2018;11(10):1904.
[25] Sahu S, Mondal DP, Cho JU, et al. Low-velocity impact characteristics of closed cell AA2014-SiCp composite foam. Compos Part B-Eng 2019;160:394–401.
[26] Saeidi Googarchin H, Pasandidehpoor M, Mahmoodi A, Shojaeefard MH. Energy absorption analysis for tapered multi-cell tubes improved by foams: Theoretical development and numerical simulation. Compos Struct 2019;207:213–22.
[27] Roszkos CS, Bocko J, Kula T, Šarloši J. Static and dynamic analyses of aluminium foam geometric models using the homogenization procedure and the FEA. Compos Part B-Eng 2019;171:361–74.
[28] Linul E, Marşavina L, Linul PA, Kovacik J. Cryogenic and high temperature compressive properties of Metal Foam Matrix Composites. Compos Struct 2019;209:490–8.
[29] Linul E, Marşavina L, Vălean C, Bănică R. Static and dynamic mode I fracture toughness of rigid PUR foams under room and cryogenic temperatures. Eng Fract Mech 2020;225:106274.
[30] Cady CM, Gray III GT, Liu C, et al. Compressive properties of a closed-cell aluminium foam as a function of strain rate and temperature. Mater Sci Eng A 2009;525(1–2):1–6.
[31] Yu YH, Choi I, Nam S, Lee DG. Cryogenic characteristics of chopped glass fiber reinforced polyurethane foam. Compos Struct 2014;107:476–81.
[32] Fiedler T, Al-Sahlani K, Linul PA, et al. Mechanical properties of A356 and ZA27 metallic syntactic foams at cryogenic temperature. J Alloys Compd 2020;813:152181.
[33] Linul E, Movahedi N, Marsavina L. The temperature and anisotropy effect on compressive behaviour of cylindrical closed-cell aluminium-alloy foams. J Alloys Compd 2018;740:1172–9.
[34] Wang P, Xu S, Li Z, et al. Temperature effects on the mechanical behaviour of aluminium foam under dynamic loading. Mater Sci Eng A 2014;599:174–9.
[35] Yang K, Yang X, Liu E, et al. Elevated temperature compressive properties and energy absorption response of in-situ grown CNT-reinforced Al composite foams. Mater Sci Eng A 2017;690:294–302.
[36] Mondal DP, Jha N, Badkul A, et al. High temperature com- pressive deformation behaviour of aluminium syntactic foam. Mater Sci Eng A 2012;534:521–9.
[37] Linul E, Lell D, Movahedi N, et al. Compressive properties of Zinc Syntactic Foams at elevated temperatures. Compos Part B-Eng 2019;167:122–34.
[38] Taherishargh M, Linul E, Broxtermann S, Fiedler T. The mechanical properties of expanded perlite-aluminium syntactic foam at elevated temperatures. J Alloy Compd 2018;737:590–6.
[39] Aakash BS, Bi S, Shields MD, Gaitanaros S. On the high-temperature crushing of metal foams. Int J Solids Struct 2019;174–175:18–27.
[40] Movahedi N, Linul E, Marsavina L. The temperature effect on the compressive behaviour of closed-cell aluminium-alloy foams. J Mater Eng Perform 2018;27(1):99–108.
[41] Orbulov IN, Szlancsik A, Kemény A, Kincses D. Compressive mechanical properties of low-cost, aluminium matrix syntactic foams. Compos Part A 2020;135:105923.
[42] Orbulov IN, Kemény A, Filep A, Gácsi Z. Compressive characteristics of bimodal aluminium matrix syntactic foams. Compos Part A 2019;124:105479.
[43] Kemény A, Leveles B, Bubonyi T, Orbulov IN. Effect of particle size and volume ratio of ceramic hollow spheres on the mechanical properties of bimodal composite metal foams. Compos Part A 2021;140:106152.
[44] Katona B, Szlancsik A, Tábi T, Orbulov IN. Compressive characteristics and low frequency damping of aluminium matrix syntactic foams. Mat Sci Eng A 2019;739:140–8.
[45] Katona B, Szebényi G, Orbulov IN. Fatigue properties of ceramic hollow sphere filled aluminium matrix syntactic foams. Mater Sci Eng A 2017;679:350–7.
[46] Simancik F, Rajner W, Laag R. Reinforced Alulight for Structural Use, In: Global symposium on materials processing and manufacturing. In: Ghosh A, Sanders TH, Claar TD, editors. Processing and properties of lightweight cellular metals and structures, TMS, Seattle, 25-34; 2002.
[47] ISO 13314. Mechanical testing of metals - Ductility testing - Compression test for porous and cellular metals, 2011.
[48] Linul E, Vălean C, Linul PA. Compressive behaviour of aluminium microfibers reinforced semi-rigid polyurethane foams. Polymers 2018;10(12):1298.
[49] Movahedi N, Murch GE, Belova IV, Fiedler T. Manufacturing and compressive properties of tube-filled metal syntactic foams. J Alloys Compd 2020;822:153465.
[50] Linul E, Movahedi N, Marsavina L. On the lateral compressive behaviour of empty and ex-situ aluminium foam-filled tubes at high temperature. Materials 2018;11(4):554.
[51] Marsavina L, Kováčik J, Linul E. Experimental validation of micromechanical models for brittle aluminium alloy foam. Theor Appl Fract Mech 2016;83:11–8.
[52] Fiedler T, Movahedi N, York L, Broxtermann S. Functionally-Graded Metallic Syntactic foams produced via particle pre-compaction. Metals 2020;10(3):314.
[53] Badkul A, Saxena S, Mondal DP. A numerical solution to accurately predict deformation behaviour of metallic foam material up-to densification region for the possible use in composite structures. Compos Struct 2020;246:112419.
[54] Khezrzadeh O, Mirzaee O, Emadoddin E, et al. Anisotropic compressive behaviour of metallic foams under extreme temperature conditions. Materials 2020;13(10):2329.
[55] Benouali AH, Froyen L, Delerue JF, Wevers M. Mechanical analysis and microstructural characterisation of metal foams. Mater Sci Tech-Lond 2002;18:489–94.
[56] Linul E, Movahedi N, Marsavina L. The temperature effect on the axial quasi-static compressive behaviour of ex-situ aluminium foam-filled tubes. Compos Struct 2017;180:709–22.
[57] Yadav BN, Muchhala D, Singh P, et al. Synergic effect of MWCNTs and SiC addition on microstructure and mechanical properties of closed-cell Al-SiC-MWCNTs HCFs. Compos Part B 2019;172:458–71.
[58] Yadav BN, Muchhala D, Sriram S, Mondal DP. Study on activation energy and strain rate sensitivity of closed-cell aluminium hybrid composite foam. J Alloys Compd 2020;832:154860.
[59] Birla S, Mondal DP, Das S, et al. Effect of cenosphere particle size and relative density on the compressive deformation behaviour of aluminium-cenosphere hybrid foam. Mater Des 2017;117:168–77.